IEEE Access
Multidisciplinary | Rapid Review | Open Access Journal

Received November 20, 2021, accepted November 28, 2021, date of publication December 1, 2021,
date of current version December 13, 2021.

Digital Object Identifier 10.1109/ACCESS.2021.3132084

Performance of NOMA-Based mmWave D2D Networks Under Practical System Conditions

LEILA TLEBALDIYEVA[1], GALYMZHAN NAURYZBAYEV[1], (Senior Member, IEEE), SULTANGALI ARZYKULOV[2], (Member, IEEE), AND AHMED M. ELTAWIL[2], (Senior Member, IEEE)

[1]Department of Electrical and Computer Engineering, School of Engineering and Digital Sciences, Nazarbayev University, Nur-Sultan 010000, Kazakhstan
[2]Computer, Electrical and Mathematical Science and Engineering Division, King Abdullah University of Science and Technology, Thuwal 23955, Saudi Arabia

Corresponding author: Galymzhan Nauryzbayev (galymzhan.nauryzbayev@nu.edu.kz)

This work was supported in part by the Nazarbayev University Social Policy Grant, and in part by the Nazarbayev University Faculty Development Competitive Research Program under Grant 240919FD3935.

ABSTRACT This work elaborates the analysis on ergodic capacity, coverage probability, and average throughput for multi-user non-orthogonal multiple access (NOMA) based device-to-device communication networks, which operate in the millimeter-wave spectrum range and are constrained by practical system imperfections such as residual transceiver hardware impairments, imperfect channel state information, and non-ideal successive interference cancellation. More importantly, we consider that the proposed network model is limited by independent and non-identically distributed interference noises emerging from neighboring device nodes. Computationally effective and comprehensive closed-form expressions are delivered to evaluate the ergodic capacity with its upper and lower bounds, as well as coverage probability and average throughput expressions. Furthermore, the asymptotic analysis of ergodic capacity and coverage probability at high and low signal-to-noise-ratio regimes are analyzed and the corresponding closed-form expressions are presented. Valuable discussions on the fairness-based power allocation scheme for NOMA users have been provided. Moreover, a thorough Monte Carlo simulation is carried out to validate the corresponding analytical findings. Finally, simulation results have revealed that the system impairments aforementioned herein cause an ergodic capacity saturation phenomenon. Especially, interference plays a significant role as a performance limitation factor for the ergodic capacity and coverage probability.

INDEX TERMS Average throughput, coverage probability, device-to-device (D2D) communications, ergodic capacity, imperfect channel state information (CSI), millimeter-wave (mmWave), non-orthogonal multiple access (NOMA), residual transceiver hardware impairment (RTHI).

I. INTRODUCTION

One of the main aims of fifth-generation (5G) communication systems is to support connections of up to 50 billion devices by 2025 [1]. To this extent, the device-to-device (D2D) communication [2]–[4], millimeter wave (mmWave) technology [5]–[8], and non-orthogonal multiple access (NOMA) [9]–[14] (enabling concurrent device connections) can fulfill this goal. The NOMA is particularly useful for efficient utilization of network resources such as time, code, frequency, as well as radio frequency (RF) chains dedicated per user equipment (UE). For instance, the in-field trials conducted by NTT DOCOMO (Japan) and MediaTek (Taiwan) demonstrated a 2.3-times spectral efficiency (SE) improvement for smartphone-sized NOMA users in comparison to the single-user multiple-input multiple-output (MIMO) scenario [15], [16].

The associate editor coordinating the review of this manuscript and approving it for publication was Chi-Tsun Cheng.

A. RELATED WORKS

In NOMA-based D2D networks, multiple and nearby located devices' signals are compounded in the power domain to boost their SE. The D2D-empowered NOMA networks also demonstrated the increase in energy efficiency, data offloading, and ability to massively connect devices [17]. The authors in [17] studied the user-clustering and power assignment optimization in the network comprising cellular users and underlay NOMA-enabled D2D users. Next, the work [4]

presented a novel resource allocation algorithm by using a many-to-one side matching theory to achieve near-optimal sum-rate performance for underlay NOMA-based D2D networks. Moreover, the authors in [18] developed an interlay mode to accommodate power-domain multiplexing for both cellular and D2D users. Next, capacity scaling of a NOMA-D2D-based cooperative relay system for the two-user scenario was investigated in [19] over Rayleigh fading channels. To conclude, it is pertinent to mention that all the aforementioned recent works considered ideal system configurations for the NOMA-based D2D networks.

It is well-known that the RF chains considerably contribute to the cost of communication systems due to their high power consumption and cost of analog-to-digital converters (ADCs)/ digital-to-analog converters (DACs) in RF chains [20]. At the same time, low-grade transceiver equipment is often used in modern high-rate systems to reduce their CAPEX costs. This inevitably adds residual transceiver hardware impairments (RTHIs) from the phase noise [21], [22], amplifier non-linearity [23], and in-phase/quadrature-phase imbalance [24] to the received signal. The RF front-end imperfections have a more negative impact on the mmWave spectrum range than in the conventional frequency range [25] due to an inverse relationship between the transmission rate and RTHI level [26].

Although the assumption of an ideal transceiver is acceptable for systems with a low data rate, this assumption is not valid for high-speed communication systems [27]. Comparative analysis of 60 GHz commercial RF front-ends for orthogonal frequency division multiplexing (OFDM) systems was presented in [28] for intrinsic RF hardware imperfections and their effect on the system performance. Moreover, the authors proposed a practical link budget analysis to evaluate Error Vector Magnitude (EVM). According to [29], RTHI limits the capacity at the UE side with multiple antennas. Oppositely, the effects of RTHI and inter-cluster interference are less severe at the base stations that employ massive MIMO antennas. Therefore, it is essential to model the RTHI noise and interference in D2D networks.

Recent works on the RTHI, imperfect channel state information (CSI), and non-ideal successive interference cancellation (SIC) have considered the cooperative NOMA networks in [30]–[37]. For instance, the authors in [30] studied the two-user uplink NOMA-based mmWave networks and proposed a joint power control and beamforming technique. Moreover, the authors in [31] evaluated the ergodic capacity for amplify-and-forward (AF) and decode-and-forward (DF) MIMO relay systems with an arbitrary number of antennas and by considering the effect of RTHI. Similarly, a NOMA-based AF relay network constrained by RTHIs was studied in [32], where the outage probability along with the ergodic capacity performance was investigated. Moreover, the recent works [33] and [34] studied the RTHI and imperfect SIC while incorporating the energy harvesting capabilities in overlay cognitive NOMA networks over Nakagami-*m* fading environment.

It was shown that the NOMA-based system outperforms the traditional orthogonal multiple access (OMA) system at the medium-to-high signal-to-noise (SNR) regime. Similarly, an approximate expression for the ergodic capacity was provided in the recent work [35] for both cooperative and non-cooperative NOMA networks considering the RTHI, imperfect CSI [38] and non-ideal SIC [39]. The authors in [36] studied the security aspects in NOMA-based AF relay cooperative networks by considering the RTHI noise, where the exact and asymptotic outage probability and intercept probability analysis were provided. The authors in [37] studied the cooperative NOMA-based coverage probability analysis for a mmWave network given an ideal system configuration; three potential relay selection schemes were proposed to justify the advantage of the cooperative NOMA approach over the traditional OMA one.

Next, the ergodic capacity analysis for NOMA-based uplink satellite networks with randomly deployed end-users under imperfect CSI and antenna-pointing errors was studied in [40]; however, this work did not study the other system impairments. Likewise, the work [41] studied the ideal NOMA network with two end-users and presented the outage probability and approximate ergodic capacity formulas.

The authors in [42] studied a different aspect of practical system imperfection in NOMA networks such as arbitrary user mobility profile at various antenna array ranges given the short packet transmission regime. The other authors in [43] introduced the heterogeneous mobility profile to group users that move at a certain speed by using a novel NOMA orthogonal frequency space modulation. Furthermore, the authors in [44] proposed a detection method and channel estimation algorithm for sky-ground uplink NOMA, where aerial users are moving while terrestrial users are static. The proposed method improved both the channel estimation and time-varying successive interference cancellation.

It is noted that the contemporary research in the field of NOMA-based mmWave D2D networks either has studied the ideal transceiver hardware or does not consider independent and non-identically distributed (i.n.i.d.) interference noise induced by neighboring device nodes. However, the authors in [45] discussed the importance of inter-cell and intra-cell interference analysis as a main limiting factor for NOMA-based 5G networks. On the other hand, they did not present an analytical performance analysis. Moreover, the authors in [46] considered a simple yet not accurate interference noise model for underlay cognitive radio NOMA networks, where several interfering nodes are treated as a Gaussian noise by applying a central limit theorem (CLT).

To the best of the authors' knowledge, little attention has been paid to studying the impact of interference in mmWave D2D NOMA networks. This problem, as well as the other realistic system impairments (*i.e.*, RTHI and imperfect CSI/SIC), are worth being addressed in forthcoming massively connected communication systems; therefore, these issues mentioned above are the main investigation aspects of this paper.

B. MAIN CONTRIBUTION

Motivated by the abovementioned discussion, in this work, we aim to study the essential sources of system impairments that degrade the performance of multi-user NOMA-based D2D mmWave networks and develop a unified framework to evaluate their performance. For statistical RTHI modeling, we adopt the power-dependent additive white Gaussian noise (AWGN) model to describe the aggregate effect of transceiver impairments due to its analytical tractability as well as its theoretical and practical validity supported by [27], [47]–[50]. Moreover, we incorporate an analytically tractable model for i.n.i.d. interference noise terms over Nakagmai-m fading channels into our system model. To the best of the authors' knowledge, no prior work derived the closed-form expressions for the ergodic capacity and coverage probability analysis considering M i.n.i.d. interference noises. Since channel conditions and signal power of interfering nodes may vary depending on their locations, it is important to consider i.n.i.d. Gamma variates to represent channel gains of Nakagami-m channel amplitudes. The authors in [51] presented a single Gamma approximation PDF for the summation of M i.n.i.d. Gamma RVs. This work enabled us to present all channel noises (a summation of M i.n.i.d. interference, RTHI, and imperfect CSI/SIC) as a single Gamma RV. This approach substantially simplified the analysis of the proposed system model.

The key contributions of this work are summarized as

- Different from [35] and [40], we develop a practical framework for NOMA-based mmWave D2D networks while considering the compound effect of RTHI, imperfect CSI/SIC, and interference from side/back lobe antenna gains of the interfering nodes in the multi-user NOMA D2D network.
- In contrast to [35] and [41], where the authors delivered the *approximate* ergodic capacity analysis of NOMA-based networks due to the mathematical complexity of the exact analytical derivations, this work delivers compact and insightful closed-form expressions for the ergodic capacity and corresponding lower and upper bounds along with the asymptotic analysis at the high and low SNR regimes.
- Closed-form expressions for the coverage probability and average throughput have been presented in this work. To obtain deeper insights, the asymptotic behavior of the coverage probability is investigated at the high-SNR regime.
- The individual effect of each system impairment (*i.e.*, RTHI, imperfect CSI/SIC, and M i.n.i.d. interference noise) is studied separately and compared with its ideal counterpart. Given a non-ideal system configuration, the closed-form power allocation (PA) scheme is proposed to ensure fairness among NOMA users. Finally, thorough Monte-Carlo simulations validate the correctness of all derived analytical expressions and demonstrate the advantage of the NOMA-based network over the OMA one.

C. NOTATIONS AND PAPER ORGANIZATION

Throughout the paper, the expectation operator is denoted as $\mathbb{E}\{\cdot\}$, $G_{pq}^{mn}\left(z\middle|\begin{matrix}b_1,\cdots,b_q\\a_1,\cdots,a_p\end{matrix}\right)$ represents the Meijer G-function, and $X \sim \mathcal{CN}\left(\mu,\sigma^2\right)$ stands for the circularly symmetric complex Gaussian random variable (RV) X with mean μ and σ^2 variance. In addition, $F_X(\cdot)$ and $f_X(\cdot)$ symbolize the cumulative distribution function (CDF) and probability density function (PDF) of RV X, correspondingly. Moreover, $\Gamma(m,\beta)$ is an incomplete Gamma function with m fading and $\beta > 0$ scale parameters, and $\psi(\cdot)$ is the digamma function [52, (8.360.1)]. $\Pr(\mathcal{C})$ is the probability of an event $\mathcal{C}$. Gamma RV $\mathcal{X}$ with m fading and β scale parameters is denoted as $\mathcal{X} \sim Gamma(m,\beta)$.

The remainder of the paper is organized as follows. Section II defines the system model of a realistic NOMA-based mmWave D2D network limited by imperfect SIC/CSI, RTHIs, and interference. Next, Section III presents generic formulas to evaluate the ergodic capacities with its lower and upper bounds for the proposed system model. Furthermore, Section IV evaluates the ergodic capacity with its lower and upper bounds and corresponding asymptotic analysis for the NOMA-based mmWave D2D network under study over Nakagami-m fading channels. Section V presents the closed-form expression for the coverage probability and its high-SNR approximation. Section V-B showcases the closed-form expression for the average throughput formula for the system model under study. Furthermore, in Section VI, the fairness aspects of the power allocation are discussed and the closed-form solution is proposed. The main result discussions are drawn in Section VII, and Section VIII summarizes the key points of the work.

II. SYSTEM MODEL

Consider a downlink NOMA-based D2D mmWave network that uses analog beamforming to establish direct communication links for N NOMA users, denoted by $U_i, i \in \mathcal{A} = \{1, 2, \ldots, N\}$. All device nodes are equipped with MIMO antennas and non-ideal transceiver hardware. The source node (S) applies the NOMA principle to communicate with N device nodes located at distances, denoted by $d_i, i \in \mathcal{A}$. It is assumed that each reference NOMA user is surrounded by M interfering user nodes.[1] The side/back lobes of the other device nodes create interference to the end-users. A base station controller unit is employed to arbitrate the coordination and beam alignment between the communicating device nodes to avoid interference. We assume an ideal beam alignment between device nodes for analytical tractability as in [3] and [53]. This way, one can focus more on the other types of system non-idealities such as RTHI, imperfect CSI/SIC, and interference. For more details on the beam misalignment, one can refer to [54], [55].

We model the mmWave channel by using Nakagami-m fading along with analog beamformed user association as

[1]Note that the number of neighboring interfering nodes for U_i can be arbitrary.

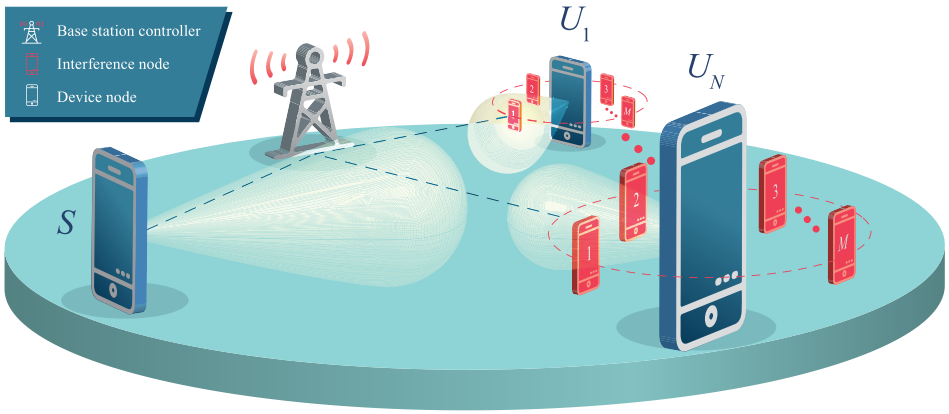

FIGURE 1. An illustration of the NOMA-based mmWave D2D network with multiple N users surrounded by M interfering nodes.

in [56] and [57], where a fading parameter m models the line-of-sight (LOS)/non-LOS components of mmWave communication. In addition, Nakagami-m distribution scaled by analog beamforming gain is a mathematically tractable solution to model mmWave channel that simplifies the analysis of complex system models.

Inspired by [53], a sectored antenna array pattern is used to model the analog beamformed antenna array as

$$G(\theta) = \begin{cases} G_s, & |\theta| > \theta_b, \\ G_m, & \text{otherwise}, \end{cases} \tag{1}$$

where θ and θ_b are the angles of a boresight direction and antenna beamwidth, accordingly. G_s and G_m indicate the gains related to the side/back and main lobes, respectively. In addition, a linear minimum mean square error is used to estimate the communication channel between S and U_i as $h_i = \tilde{h}_i + \epsilon_i$, where h_i, $\tilde{h}_i$, and ϵ_i denote the channel amplitude, estimated channel amplitude, and estimation error with $\epsilon_i \sim \mathcal{CN}\left(0, \sigma_{ei}^2\right)$, respectively, where σ_{ei}^2 approximates the error in the channel estimation. The NOMA technology allows S to transmit a superimposed signal $x = \sum_{n=1}^{N} \sqrt{\alpha_n P} x_n$ towards N NOMA nodes, where x_n is the signal designated for the nth user, α_n is the PA coefficient with a unit power property, given by $\sum_{n=1}^{N} \alpha_n = 1$, and P is the average signal power. The PA coefficient ensures fairness during the power allocation process for U_i. In this paper, similar to [58], we allocate the power based on the quality of service (QoS) requirements imposed on the NOMA users. For example, a higher PA coefficient is assigned to a user with a higher QoS requirement, while a user with a lower QoS is devoted to a smaller PA coefficient. Therefore, we order the PA factors for the NOMA users as $\alpha_1 > \alpha_2 > \ldots > \alpha_n > \ldots > \alpha_N$.

Hence, the received signal at a reference receiver, U_i, is given as

$$r_i = \sqrt{G_m^2 d_i^{-\tau}} h_i \left(\sum_{n=1}^{N} \sqrt{\alpha_n P} x_n + \mu_i \right) + \sum_{k=1}^{M} \sqrt{G_s G_k d_{ik}^{-\tau'}} g_{ik} \left(\sqrt{I_k} s_k + \bar{\mu}_k \right) + w_i, \tag{2}$$

where τ is the path loss exponent (PLE) of the main D2D link, τ' is the PLE of the interference links,[2] d_i and d_{ik} are the distances between S to U_i and between U_i to interfering node k, respectively. Moreover, G_k is a gain factor from an interfering node k, which can either land to the reference receiver's side/back lobe with the main lobe or side/back lobe (G_m or G_s). In (2), h_i is the channel between the D2D pair, while g_{ik} is the channel between the kth interference node and the reference receiver i within a given cluster, h_i and g_{ik} are both Nakagami-m distributed channel amplitudes. Additionally, I_k is the average signal power from the interfering node k, RTHI noise components are modeled as $\mu_i \sim \mathcal{CN}\left(0, \kappa_i^2 P\right)$ and $\bar{\mu}_k \sim \mathcal{CN}\left(0, \bar{\kappa}_k^2 I_k\right)$, where κ_i and $\bar{\kappa}_k$ are the RTHI levels measured by EVM [59]. The EVM metric is frequently applied to measure a mismatch between intended and actual signals. An ideal RF transceiver would have an EVM value equal to zero and lower values of EVM signify a higher quality of RF transceiver hardware [32]. Moreover, $w_i \sim \mathcal{CN}\left(0, \sigma_i^2\right)$ is the AWGN term. Furthermore, the signal-to-interference-noise-distortion ratio (SINDR) at U_i to decode the signal x_j given $j \leq i$ can be formulated by considering the RTHI, interference, and imperfect CSI/SIC as

$$\gamma_j^{[i]} = \frac{\alpha_j \rho_i |\tilde{h}_i|^2}{\rho_i \mathcal{B}_j |\tilde{h}_i|^2 + \Lambda^{[i]} + \sum_{k=1}^{M} |g_{ik}|^2 \left(1 + \bar{\kappa}_k^2\right) \bar{\rho}_{ik}}, \tag{3}$$

where $\rho_i = P G_m^2 d_i^{-\tau}$, $\bar{\rho}_{ik} = I_k G_s G_k d_{ik}^{-\tau}$, and $\Lambda^{[i]} = \sigma_i^2 + \rho_i \left(1 + \kappa_i^2\right) \sigma_{ei}^2$. Next, $\mathcal{B}_j = \left(\Phi_j + \tilde{\Phi}_j + \kappa_i^2\right)$, where $\Phi_j = \sum_{t=j+1}^{N} \alpha_t$ and $\tilde{\Phi}_j = \sum_{r=1}^{j-1} \xi_r \alpha_r$ for imperfect SIC range, $0 \leq \xi_r \leq 1$, such that $\xi_r = 0$ represents ideal SIC and $\xi_r = 1$ stands for non-ideal SIC. We make the following variable

[2]It is reasonable to assume the equality of the PLE values, *i.e.*, $\tau = \tau'$.

substitutions for simplification purposes of SINDR as

$$\gamma_j^{[i]} = \frac{a_j^{[i]} X^{[i]}}{b_j^{[i]} X^{[i]} + Z^{[i]} + \Lambda^{[i]}}, \tag{4}$$

where $X^{[i]} = |\tilde{h}_i|^2$, $\zeta_k^{[i]} = \left(1 + \bar{\kappa}_k^2\right) \bar{\rho}_{ik}$, $Z^{[i]} = \sum_{k=1}^{M} Y_k^{[i]} = \sum_{k=1}^{M} |g_{ik}|^2 \zeta_k^{[i]}$, $a_j^{[i]} = \alpha_j \rho_i$ and $b_j^{[i]} = \rho_i \left(\Phi_j + \tilde{\Phi}_j + \kappa_i^2\right)$. Note that U_1 decodes its own signal x_1 and treats other x_n messages as a noise with $\Phi_1 = \sum_{t=2}^{N} \alpha_t$ and $\tilde{\Phi}_1 = 0$ parameters. The user U_N decodes the x_N signal by applying SIC and by evaluating $\tilde{\Phi}_N = \sum_{r=1}^{N-1} \xi_r \alpha_r$.

III. GENERIC ERGODIC CAPACITY WITH BOUNDS

This section analyzes the ergodic capacity of NOMA-based mmWave D2D networks by considering RTHI, imperfect CSI/SIC, and i.n.i.d. interference noises. Inspired by [60], the general expressions for the ergodic capacity with its upper and lower bounds for a NOMA-based mmWave D2D network constrained by system imperfections in arbitrary fading channels are formulated below.

A. ERGODIC CAPACITY

By definition, the ergodic capacity is given by

$$\begin{aligned} C_j^{[i]} &= \mathbb{E}\left\{ \log_2 \left(1 + \gamma_j^{[i]}\right) \right\} \\ &= \mathbb{E}\left\{ \log_2 \left(1 + \frac{a_j^{[i]} X^{[i]}}{\Lambda^{[i]} + Z^{[i]} + b_j^{[i]} X^{[i]}}\right) \right\}. \end{aligned} \tag{5}$$

By using the property of a logarithm function, (5) can be further written as a difference of two terms

$$\begin{aligned} C_j^{[i]} = \mathbb{E}\left\{ \log_2 \left(X^{[i]}(a_j^{[i]} + b_j^{[i]}) + \Lambda^{[i]} + Z^{[i]}\right) \right\} \\ - \mathbb{E}\left\{ \log_2 \left(\Lambda^{[i]} + Z^{[i]} + b_j^{[i]} X^{[i]}\right) \right\}. \end{aligned} \tag{6}$$

We make the following variable substitutions in (6) for simplification purposes: $T^{[i]} = X^{[i]}(a_j^{[i]} + b_j^{[i]}) + Z^{[i]}$ that represents the summation of $(M + 1)$ i.n.i.d. Gamma RVs and $V^{[i]} = b_j^{[i]} X^{[i]} + Z^{[i]}$ is another summation of $(M + 1)$ i.n.i.d. Gamma RVs with different fading and scale parameters. Hence, we get the following simplified representation for the ergodic capacity as

$$C_j^{[i]} = \mathbb{E}\left\{ \log_2 \left(\Lambda^{[i]} + T^{[i]}\right) \right\} - \mathbb{E}\left\{ \log_2 \left(\Lambda^{[i]} + V^{[i]}\right) \right\}. \tag{7}$$

B. LOWER ERGODIC CAPACITY

By using the concavity property of $\log_2(1 + \upsilon \exp(x))$ for variable x with $\upsilon > 0$ and Jensen's inequality [52, (12.41)], the ergodic capacity is lower-bounded as

$$\begin{aligned} C_j^{L[i]} &= \log_2 \left(1 + \exp\left(\mathbb{E}\left\{\ln\left(\gamma_j^{[i]}\right)\right\}\right)\right) \\ &= \log_2 \left(1 + \exp\left(\mathbb{E}\left\{\ln\left(\frac{a_j^{[i]} X^{[i]}}{\Lambda^{[i]} + V^{[i]}}\right)\right\}\right)\right). \end{aligned} \tag{8}$$

Next, by exploiting the property of a logarithmic function, we can rewrite the lower bound ergodic capacity as

$$\begin{aligned} C_j^{L[i]} = \log_2 \left(1 + \exp\left(\mathbb{E}\left\{ \ln(a_j^{[i]} X^{[i]})\right\}\right.\right. \\ \left.\left. - \mathbb{E}\left\{ \ln(\Lambda^{[i]} + V^{[i]})\right\}\right)\right). \end{aligned} \tag{9}$$

C. UPPER ERGODIC CAPACITY

Since a logarithm is a concave function, Jensen's inequality is applied to evaluate the generic upper ergodic capacity as

$$\begin{aligned} C_j^{U[i]} &= \log_2 \left(1 + \mathbb{E}\left\{\gamma_j^{[i]}\right\}\right) \\ &= \log_2 \left(1 + \mathbb{E}\left\{\frac{a_j^{[i]} X^{[i]}}{\Lambda^{[i]} + V^{[i]}}\right\}\right) \\ &= \log_2 \left(1 + a_j^{[i]} \mathbb{E}\left\{X^{[i]}\right\} \mathbb{E}\left\{\frac{1}{\Lambda^{[i]} + V^{[i]}}\right\}\right). \end{aligned} \tag{10}$$

IV. ERGODIC CAPACITY WITH BOUNDS IN NAKAGAMI-*m* FADING CHANNEL

This section demonstrates the approximated closed-form expressions for the ergodic capacity with its upper and lower bounds in for NOMA-based mmWave D2D network with system impairments over Nakagami-*m* fading channels.

Lemma 1 below closely approximates PDF of a summation of Q i.n.i.d. Gamma variates. Its proof and validation are presented in detail by the authors in [51]. The ergodic capacity and ergodic capacity bounds are evaluated with the aid of *Lemma 1*.

Lemma 1: Consider $X_t \quad (t = 1, \cdots, Q)$ are non-negative i.n.i.d. Gamma RVs with m_t fading and β_t scale parameters, accordingly. The probability density function (PDF) of $Z = \sum_{t=1}^{Q} X_t$ is given as

$$f_Z(z) = \frac{z^{\tilde{m}_z - 1} \exp\left(-\frac{z}{\tilde{\beta}_z}\right)}{\Gamma(\tilde{m}_z) \tilde{\beta}_z^{\tilde{m}_z}}, \tag{11}$$

where an approximated scale parameter of a single Gamma function, $\tilde{\beta}$, is evaluated by solving a set of equations $\frac{\mu}{2} - 2\sum_{t=1}^{Q} \frac{m_t \beta_t^3}{(\beta_t + \tilde{\beta}_z)^2} = 0$ and $\mu = \sum_{t=1}^{Q} m_t \beta_t$. A shape parameter for the single Gamma function is evaluated from $\tilde{m}_z = \frac{\mu}{\tilde{\beta}_z}$.

We derive an ergodic capacity with the aid of *Lemma 1* to represent the summation of $(M + 1)$ i.n.i.d. Gamma variates.

Proposition 1: The ergodic capacity for a NOMA-based mmWave D2D network in an analog beamformed Nakagami-*m* fading channel with RTHI, imperfect CSI/SIC, and M i.n.i.d. interference constraints is given by

$$\tilde{C}_j^{[i]} = \frac{G_{3,2}^{1,3}\left(\frac{\hat{\beta}_t}{\Lambda^{[i]}} \middle| \begin{matrix} 1-\hat{m}_t, 1, 1 \\ 1, 0 \end{matrix}\right)}{\ln(2)\Gamma(\hat{m}_t)} - \frac{G_{3,2}^{1,3}\left(\frac{\hat{\beta}_v}{\Lambda^{[i]}} \middle| \begin{matrix} 1-\hat{m}_v, 1, 1 \\ 1, 0 \end{matrix}\right)}{\ln(2)\Gamma(\hat{m}_v)}, \tag{12}$$

where $\{\hat{\beta}_t, \hat{\beta}_v\}$ and $\{\hat{m}_t, \hat{m}_v\}$ are the scale and fading parameters of $T^{[i]} \sim \Gamma(\hat{m}_t, \hat{\beta}_t)$ and $V^{[i]} \sim \Gamma(\hat{m}_t, \hat{\beta}_t)$ single

Gamma representations of the sum of $(M+1)$ i.n.i.d. Gamma distributed noise components, accordingly.

Proof: Full proof is relegated to Appendix A. ■

There are the other PDFs available that could be used to represent a summation of M i.n.i.d. Gamma variates. For instance, the work in [61] developed a summation PDF in terms of Fox H-function, which is mathematically very challenging to be integrated into the computation of ergodic capacity. In fact, the author in [62] represented the PDF for summation of M i.n.i.d. Gamma RVs as the semi-infinite summations with a recursive function. However, it is computationally intensive to use this PDF in our system model as well. It is possible to derive the compact ergodic capacity formula by using a single Gamma representation for the summation of M i.n.i.d. Gamma RVs [51].

Proposition 2 below presents a closed-form expression for the lower bound of ergodic capacity.

Proposition 2: The ergodic capacity for a NOMA-based mmWave D2D network with RTHI, imperfect CSI/SIC, and interference noise is lower bounded by

$$\tilde{C}_j^{L[i]} = \log_2\left(1+\exp\left(\ln(a_j^{[i]}\beta_i)+\psi(m_i)-\ln(\Lambda^{[i]}) -G_{3,2}^{1,3}\left(\frac{\hat{\beta}_v}{\Lambda^{[i]}}\middle|\begin{matrix}1-\hat{m}_v,1,1\\1,0\end{matrix}\right)\right)\right). \quad (13)$$

Proof: See Appendix B. ■

Similarly, *Proposition 3* presents an upper ergodic capacity for the proposed system model.

Proposition 3: An upper bound of the ergodic capacity for a given NOMA-based mmWave D2D network with system impairments and M interference noise terms is evaluated by using (10) as

$$\tilde{C}_j^{U[i]} = \log_2\left(1+a_j^{[i]}\beta_i m_i\hat{\beta}_v^{-\hat{m}_v}\Lambda^{[i]-1+\hat{m}_v}\exp\left(\frac{\Lambda^{[i]}}{\hat{\beta}_v}\right) \times\Gamma\left(1-\hat{m}_v,\frac{\Lambda^{[i]}}{\hat{\beta}_v}\right)\right). \quad (14)$$

Proof: The proof is relegated to Appendix C. ■

A. ASYMPTOTIC ANALYSIS

System imperfection noises, such as RTHI and imperfect CSI/SIC, are proportional to the transmit power. Therefore, it is particularly interesting to analyze the ergodic capacity at the high-SNR regime to elaborate their effect on the capacity ceiling. *Proposition 4* below provides the closed-form expression for asymptotic ergodic capacity formulas at the high-SNR regime.

Proposition 4: The asymptotic ergodic capacity formula for the proposed NOMA-based mmWave D2D network at high-SNR regime is evaluated as

$$\lim_{\mathrm{SNR}_i\to\infty}\tilde{C}_j^{[i]} = \log_2\left(1+\frac{\alpha_j\beta_i m_i}{(1+\kappa_i^2)\sigma_{ei}^2+\mathcal{B}_j\beta_i m_i}\right). \quad (15)$$

Proof: The proof is in Appendix D. ■

Next, by using the SINDR in terms of SNR_i given in (D.2) and by taking the limit of the ergodic capacity when SNR tends to zero, we obtain low-SNR ergodic capacity

$$\lim_{\mathrm{SNR}_i\to 0}\tilde{C}_j^{[i]} = \log_2(1+0)\approx 0. \quad (16)$$

The ergodic capacity in the high-SNR regime is particularly important to verify whether the system impairments contribute to limit the performance of high-rate systems.

V. COVERAGE PROBABILITY

In the following section, the coverage probability analysis for the proposed system model has been performed. The coverage probability evaluates the probability of the received signal, x_j being correctly decoded at the reference receiver, U_i, which is calculated by the probability of the SINDR being higher at the predefined rate threshold, $v = 2^{R_{th}}-1 > 0$, where R_{th} is the communication rate threshold.

$$P_c^{[i]}(v) = \Pr\left(\gamma_j^{[i]} > v\right), \quad 0 < j \leqslant i, i \in N. \quad (17)$$

Proposition 5: For NOMA-based mmWave D2D network constrained by N i.n.i.d. interference, imperfect CSI/SIC, and RTHI, coverage probability is evaluated by applying (17) and *Lemma 1* to approximate the summation of N interference noise as a single Gamma RV and shown at the bottom of the page, where $\omega_i = \frac{v}{\beta_i\left(\Lambda^{[i]}-vb_j^{[i]}\right)}$.

Proof: A full derivation is shown in Appendix E. ■

A. ASYMPTOTIC ANALYSIS: HIGH-SNR APPROXIMATION

In this subsection, we present the coverage analysis using asymptotic high-SNR behaviour for the NOMA-based mmWave D2D networks under interference noise, RTHI, and imperfect CSI/SIC. By considering the high-SNR regime for (D.3), the asymptotic coverage probability is evaluated as

$$\tilde{P}_c^{[i]}(v) = \Pr\left(\tilde{\gamma}_j^{[i]} > v\right) = \Pr\left(X^{[i]} > \frac{v(1+\kappa_i^2\sigma_{ei}^2)}{\alpha_j - v\mathcal{B}_j}\right)$$

$$P_c^{[i]}(v) = \begin{cases} \sum_{t=0}^{m_i-1}\frac{\omega_i^t}{\Gamma(\tilde{m}_t)\tilde{\beta}_t^{\tilde{m}_t}}\sum_{k=0}^{t}\frac{\Lambda^{[i]t-k}}{k!(t-k)!}(\omega_i+\frac{1}{\tilde{\beta}_t})^{-k-\tilde{m}_t}\exp(-\omega_i\Lambda^{[i]})\Gamma(k+\tilde{m}_t), & 0\leq v<\frac{a_j^{[i]}}{b_j^{[j]}} \\ 0, & v>\frac{a_j^{[i]}}{b_j^{[i]}} \end{cases} \quad (18)$$

$$= 1 - F_{X^{[i]}}\left(\frac{v\left(1+\kappa_i^2\sigma_{ei}^2\right)}{\alpha_j - v\mathcal{B}_j}\right), \tag{19}$$

where $X^{[i]} \sim Gamma(m_i, \beta_i)$ and generic CDF of Gamma RV $X^{[i]}$ is given as $F_{X^{[i]}}(x) = \frac{\gamma\left(a,\frac{x}{b}\right)}{\Gamma(a)}$, that can be represented in a series form as

$$F_{X^{[i]}}(x;a,b) = 1 - \exp\left(-\frac{x}{b}\right)\sum_{t=0}^{a-1}\frac{\left(\frac{x}{b}\right)^t}{t!}. \tag{20}$$

Next, by using (19) and (20), the asymptotic coverage probability at high-SNR region is given as

$$\tilde{P}_c^{[i]}(v) = \exp\left(-\frac{v(1+\kappa_i^2\sigma_{ei}^2)}{(\alpha_j - v\mathcal{B}_j)\beta_i}\right) \times \sum_{t=0}^{m_i-1}\left(\frac{v(1+\kappa_i^2\sigma_{ei}^2)}{(\alpha_j - v\mathcal{B}_j)\beta_i}\right)^t \frac{1}{t!}. \tag{21}$$

B. AVERAGE THROUGHPUT ANALYSIS

In this subsection, the average throughput evaluation formula is given for the NOMA-based mmWave D2D network under system impairments.

Proposition 6: Consider a NOMA-based mmWave D2D network that is constrained by RTHI, imperfect CSI/SIC noise, and i.n.i.d. interference noise. The average throughput formula is given as

$$R^{[i]} = \sum_{t=0}^{m_i-1}\frac{\omega_i^t}{\Gamma(\tilde{m}_t)\tilde{\beta}_t^{\tilde{m}_t}}\sum_{k=0}^{t}\frac{\Lambda^{[i]t-k}}{k!(t-k)!}\left(\omega_i + \frac{1}{\tilde{\beta}_t}\right)^{-k-\tilde{m}_t} \times \left(\frac{G_{3,2}^{1,3}\left(\frac{\hat{\beta}_t}{\Lambda^{[i]}}\middle|\begin{matrix}1-\hat{m}_t,1,1\\1,0\end{matrix}\right)}{\ln(2)\Gamma(\hat{m}_t)} - \frac{G_{3,2}^{1,3}\left(\frac{\hat{\beta}_v}{\Lambda^{[i]}}\middle|\begin{matrix}1-\hat{m}_v,1,1\\1,0\end{matrix}\right)}{\ln(2)\Gamma(\hat{m}_v)}\right) \times \exp\left(-\omega_i\Lambda^{[i]}\right)\Gamma\left(k+\tilde{m}_t\right). \tag{22}$$

Proof: By definition, the average throughput is the multiplication of the ergodic capacity by the coverage probability as $R^{[i]} = \mathbb{E}\left\{\log_2\left(1+\gamma_j^{[i]}\right)\right\}P_c^{[i]}$ [63]. Hence, the average throughput closed-form expression is found by multiplying (12) and (17) that stand for the ergodic capacity and coverage probability, correspondingly. ■

VI. FAIRNESS-BASED POWER ALLOCATION

In addition to the presented comprehensive performance analysis, in this section, we obtain a closed-form adaptive PA solution based on the fair treatment of NOMA users to provide them with equal ergodic capacity/coverage/throughput metrics to NOMA users. The previously derived analytical findings on the ergodic capacity, coverage probability, and average throughput performance metrics are based on fixed pa factors, where users are allocated power depending on their channel conditions. Hence, users obtain different ergodic capacity and coverage probability results. The more obvious way of finding the optimal PA for NOMA users is to retrieve them from the closed-form expressions of ergodic capacity in (12) and coverage probability in (18). However, due to the complexity of those equations, the derivation of optimal PAs becomes very challenging or even intractable. Therefore, we equalize the SINDR values of NOMA users to the optimal SINDR, denoted by $\ddot{\gamma}$. It is pertinent to note that NOMA is recommended for use only in the case of two users since the NOMA-induced processing complexity non-linearly depends on the number of active user devices [64]. The system complexity aspects become more essential when the SIC-caused error propagation happens [65]. Moreover, we show in Fig. 2 that NOMA networks provide the best capacity performance for $N = 2$ compared to the cases when $N > 2$. With that, the design of a closed-form optimal PA scheme becomes infeasible for the considered system model, with $N > 2$. Hence, considering above-mentioned discussions, we provide a closed-form optimal PA solution for a two-user case with γ_1 and γ_2. Thus, to find the optimal PA and SINDR, we formulate the problem as follows

$$\underset{\Psi}{\text{minimize}} \quad |\gamma_1 - \gamma_2| \geq \Psi \tag{23a}$$

$$\text{subject to} \quad \gamma_i = \ddot{\gamma},\ \forall i \in \{1,2\} \tag{23b}$$

$$\sum_{i=1}^{2}\alpha_i \leq 1. \tag{23c}$$

The corresponding solution for (23a) is found by making $\gamma_1 = \ddot{\gamma}$ and $\gamma_2 = \ddot{\gamma}$, which can be written as

$$\frac{\alpha_1\rho_1|\tilde{h}_1|^2}{\rho_1|\tilde{h}_1|^2(\alpha_2+\kappa_1^2) + \Lambda^{[1]} + Z^{[1]}} = \ddot{\gamma}, \tag{24}$$

$$\frac{\alpha_2\rho_2|\tilde{h}_2|^2}{\rho_2|\tilde{h}_2|^2(\xi_1\alpha_1+\kappa_2^2) + \Lambda^{[2]} + Z^{[2]}} = \ddot{\gamma}. \tag{25}$$

Then, from (24) and (25), we derive α_1 and α_2 as

$$\alpha_1 = \ddot{\gamma}\alpha_2 + \ddot{\gamma}\bar{I}_1, \tag{26}$$

$$\alpha_2 = \ddot{\gamma}\xi_1\alpha_1 + \ddot{\gamma}\bar{I}_2, \tag{27}$$

where $\bar{I}_i = \frac{I_i}{|\tilde{h}_i|^2}$ and $I_i = \kappa_i^2|\tilde{h}_i|^2 + \frac{\Lambda^{[i]}+Z^{[i]}}{\rho_i}$, with $\forall i \in \{1,2\}$. Then, after substituting (27) into (26), α_1 can be written as a function of $\ddot{\gamma}$ as

$$\alpha_1 = \frac{\ddot{\gamma}^2\bar{I}_2 + \ddot{\gamma}\bar{I}_1}{1 - \ddot{\gamma}^2\xi_1}. \tag{28}$$

Now, substituting (28) into (27), α_2 can be rewritten as a function of $\ddot{\gamma}$ as

$$\alpha_2 = \frac{\ddot{\gamma}^3\xi_1\bar{I}_2 + \ddot{\gamma}^2\xi_1\bar{I}_1}{1 - \ddot{\gamma}^2\xi_1} + \ddot{\gamma}\bar{I}_2. \tag{29}$$

Furthermore, after inserting (28) and (29) into $\alpha_1 + \alpha_2 \leq 1$ and after some mathematical manipulations, the optimal SINDR can be written as

$$\ddot{\gamma} = \frac{\sqrt{(\bar{I}_1+\bar{I}_2)^2 - (\bar{I}_1+\bar{I}_2) - 4(\bar{I}_2 + \bar{I}_1\xi_1 + \xi_1)}}{2(\bar{I}_2 + \bar{I}_1\xi_1 + \xi_1)}. \tag{30}$$

Finally, we obtain optimal α_1 and α_2 by inserting (30) into (28) and (29), respectively.

VII. RESULTS DISCUSSION

This section provides some numerical examples to corroborate our analytical derivations on the ergodic capacity, coverage probability, and average throughput under different levels of system imperfections such as RTHI, imperfect CSI/SIC, and i.n.i.d. interference noise. These findings are fully validated through the averaged results via Monte-Carlo simulation. We assume the following simulation parameters unless it stated otherwise: each reference U_i is surrounded by M interference users that are located at different radial distances,[3] *i.e.*, $d_{ik} = \{8; 15; 22\}$ m, from U_i; all device nodes are equipped with $L = 16$ antennas that produce a main lobe gain of $G_m = L = 16$ in linear scale (or $G_m = 12$ in dB scale) and a side lobe gain calculated using $G_s = 0.7746 = -1.1092$ dB [3, Table 1]; all channel links are LOS and interfering nodes hit the side lobes of the reference U_i either by the main or side lobes; an equal ratio of main and side lobes of interferers; finally, the remaining simulation parameters are drawn in Table 1, which mostly follow the ones in [35], [39], [66]. The Figs. 2-7 and Figs. 9-15 are plotted as a function of transmit SNR by setting the AWGN noise variance to $\sigma_i^2 = -80$ dBm as in [67], [68]. To obtain a full vision on the system performance, we study both fixed (in Figs. 2-8) and fair, that is, adaptive, (in Figs. 9-15) PA schemes. The selection of the fixed or fair PA schemes is a matter of the system preferences.

TABLE 1. Simulation parameters.

Parameter	Value
LOS/NLOS fading parameter, m_i	$\{4; 2\}$
LOS fading parameter at U_k, $m_k, k \in \{1, \cdots, M\}$	4
The PA factors, $N = 2$, $\{\alpha_1, \alpha_2\}$	$\{0.8, 0.2\}$
PLE for LOS/ PLE for NLOS, τ	$\{2; 4\}$
PLE for LOS at U_k, τ'	2
Distance from S to U_1, d_1	100 m
Distance from S to U_2, d_2	50 m
Main lobe antenna gain, G_m	12 dB
Side/back lobe antenna gain, G_s	-1.1092 dB
Radius of the clusters, R	30 m
Interference-to-noise power ratio, I/σ_i^2	15 dB

A. FIXED POWER ALLOCATION

In Fig. 2, we evaluate the sum-rate of normalized ergodic capacity both for the multi-user NOMA and multi-user OMA networks with $N = \{2, 3, 4\}$ users for ideal system parameters (given by $\kappa_i = 0$, $\sigma_{ei}^2 = 0$ and $\xi_i = 0$) in the presence of $M = 24$ i.n.i.d. interfering nodes. In this figure, we assume the fixed PA coefficients for the two-user NOMA network are set to $\alpha_1 = 0.8$ and $\alpha_2 = 0.2$ [35], whereas, for the three and four-user NOMA networks, the fixed power coefficients are evaluated as $\alpha_i = \frac{2^{N-i}P}{2^N-1}$. Based on this figure, one can witness a minor advantage of the two-user NOMA network at the mid-SNR region as opposed to the

[3]This geometry for interfering nodes is simulation-specific; however, the closed-form expressions for performance metrics are valid for any fixed location of i.n.i.d. interfering nodes. The users' distribution is beyond the scope of this paper.

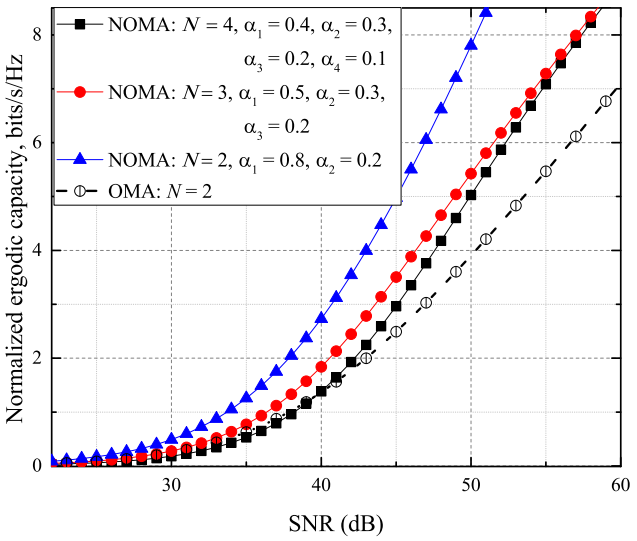

FIGURE 2. Sum-rate of normalized ergodic capacity for NOMA and OMA networks with $N = \{2, 3, 4\}$ users for the ideal system model under AWGN and interference noises.

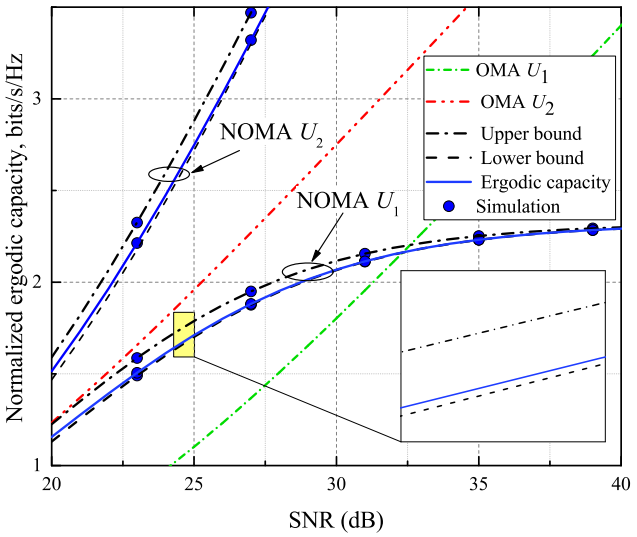

FIGURE 3. Normalized ergodic capacity with upper and lower bounds for ideal system model under AWGN and interference noises.

$N = 3$ and $N = 4$ counterparts. To support this, the authors in [35] also demonstrated that the NOMA networks have the best performance for the two-user case. Therefore, we will carry out further numerical analysis for the two-user NOMA network. Similarly, the two-user OMA network also performs better than the three- and four-user OMA networks. From Fig. 2, the overall ergodic capacity for the two-user NOMA network performs higher than the two-user OMA network. For example, at the transmit SNR of 50 and 60 dB, the sum-rate of ergodic capacity for the NOMA network achieves 5.55 and 8.96 bits/s/Hz, whereas the OMA network supports 4 and 7 bits/s/Hz, respectively.

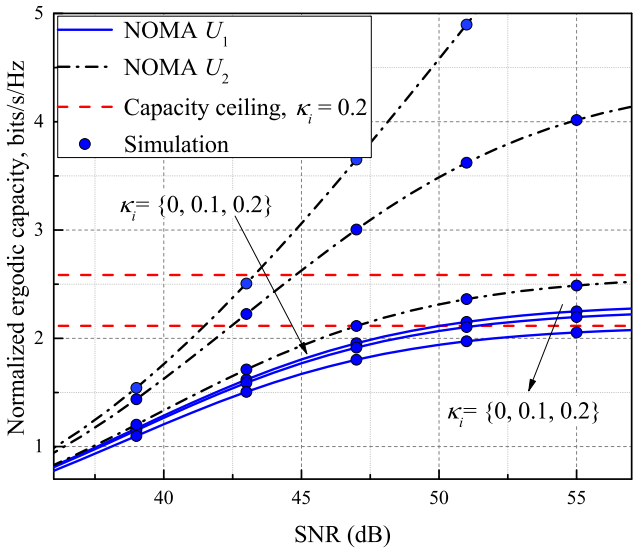

FIGURE 4. Normalized ergodic capacity for NOMA U_1/U_2 at $\kappa_i = \{0, 0.1, 0.2\}$, $\sigma^2_{ei} = 0$, $\xi_i = 0$, and $M = 24$.

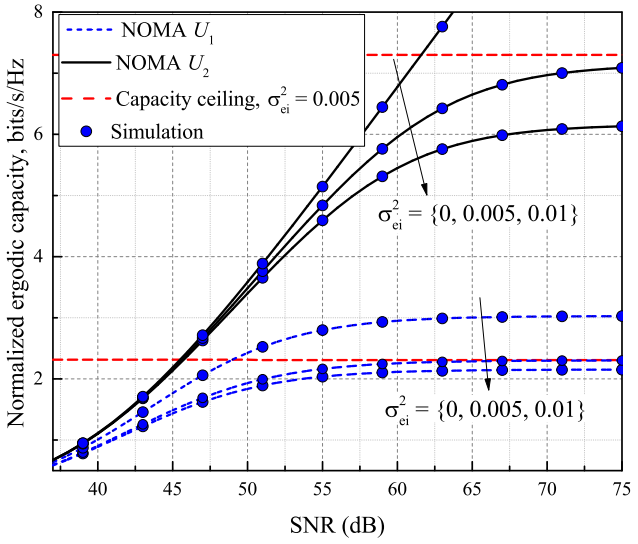

FIGURE 5. Normalized ergodic capacity for NOMA U_1/U_2 at $\sigma^2_{ei} = \{0, 005, 0.01\}$, $\kappa_i = 0$, $\xi_i = 0$, and $M = 24$.

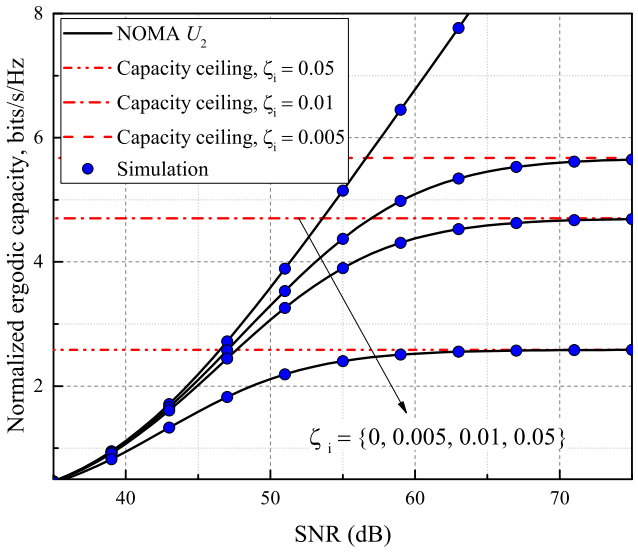

FIGURE 6. Normalized ergodic capacity at $\kappa_i = 0$, $\sigma^2_{ei} = 0$, $\xi_i = \{0, 0.005, 0.01, 0.05\}$, and $M = 24$.

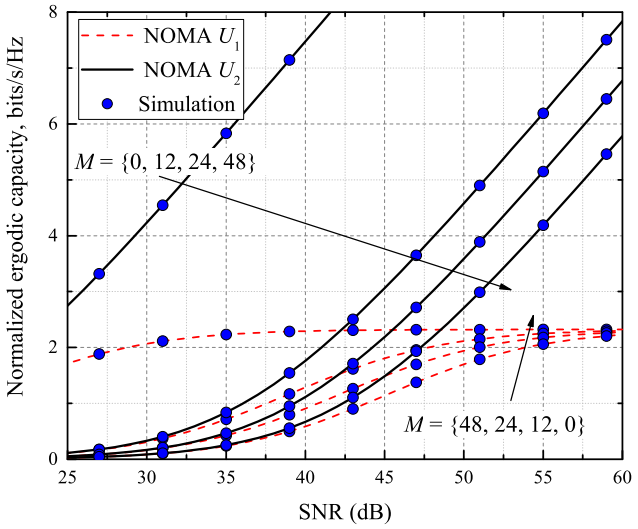

FIGURE 7. Normalized ergodic capacity at $\xi_i = 0$, $\kappa_i = 0$, $\sigma^2_{ei} = 0$, and $M = \{0, 12, 24, 48\}$.

In Fig. 3, we make a comparison of the normalized ergodic capacities between NOMA U_1/U_2 and OMA[4] U_1/U_2 users as the transmit SNR ranges from 20 to 40 dB in an ideal NOMA network with ideal transceiver hardware, perfect CSI/SIC, as well as under the presence of AWGN and interference, *i.e.*, $\kappa_i = 0$, $\sigma^2_{ei} = 0$, $\xi_i = 0$, and $M = 24$. From the NOMA results, one can notice that U_2 outperforms U_1 which can be explained by the SIC implementation at U_2. At the same time, U_1 experiences saturation above the transmit SNR of 25 dB since the signal of U_2 contributes to the SINDR of U_1 as an additional noise power, and it has the more substantial effect at higher SNR values. Compared to the OMA users, the NOMA ones are characterized by higher ergodic capacity, *i.e.*, NOMA U_2 outperforms OMA U_2 by at least 1 bits/s/Hz while NOMA U_1 outperforms OMA U_1 up to 32.5 dB. However, when the transmit SNR increases further, OMA U_1 starts outperforming NOMA U_1 mainly due to the interference caused by NOMA U_2. Fig. 3 also presents the plots for the lower and upper bounds for the ergodic capacity for NOMA U_1/U_2. The lower and upper bounds of ergodic capacity are tight to ergodic capacity. Therefore, these formulas can be alternatively used to analyze the ergodic capacity accurately.

[4]Note that the OMA users are assumed to operate in TDMA mode, when each user transmits in a dedicated time slot. Therefore, the ergodic capacity for OMA $U_{i|i\in\{N\}}$ is evaluated as $U_i^{OMA} = \frac{1}{N}\log_2(1+\gamma_j^{[i]})$.

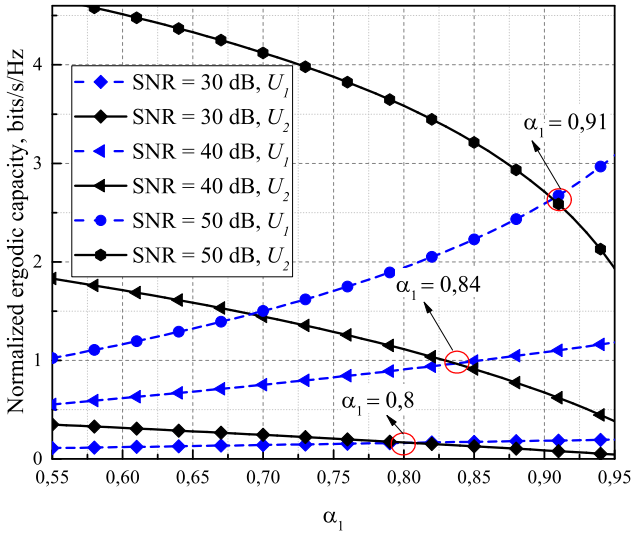

FIGURE 8. Normalized ergodic capacity of NOMA U_1/U_2 at $\xi_i = 0$, $\kappa_i = 0$, $\sigma^2_{ei} = 0$, $M = 24$, and SNR = {30, 40, 50} dB.

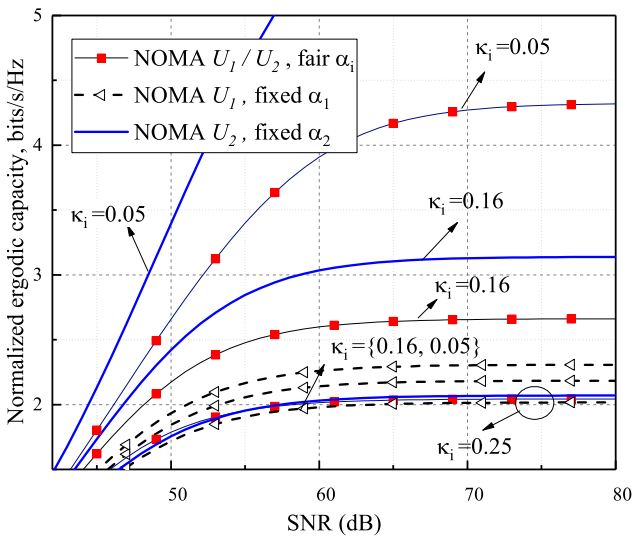

FIGURE 9. Normalized ergodic capacity at κ_i = {0.05, 0.16, 0.25}, $\xi_i = 0$, $\sigma^2_{ei} = 0$, $M = 24$ with/without user fairness.

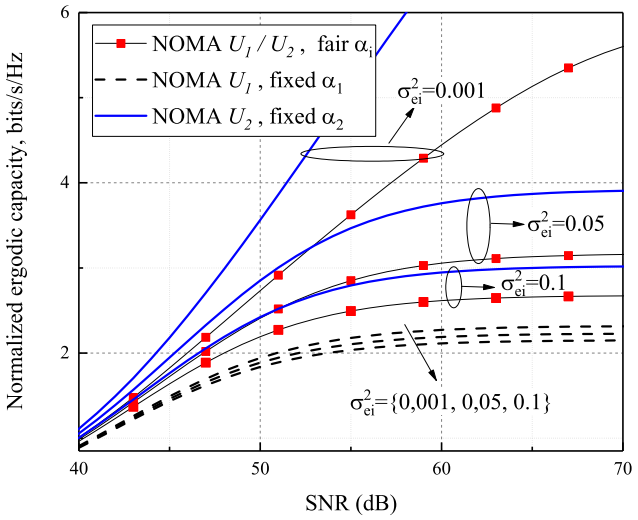

FIGURE 10. Normalized ergodic capacity at σ^2_{ei} = {0.001, 0.05, 0.1}, $\kappa_i = 0$, $\xi_i = 0$, $M = 24$ with and without user fairness.

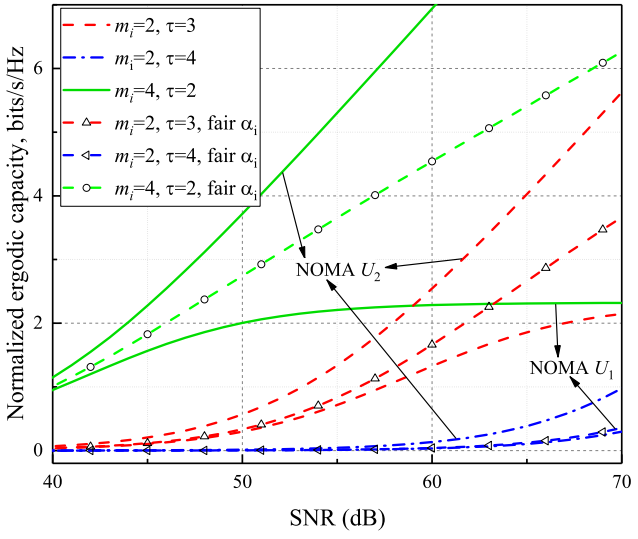

FIGURE 11. Normalized ergodic capacity at $\xi_i = 0$, $\kappa_i = 0$, $\sigma^2_{ei} = 0$, $M = 24$, and m_i = {4, 2} for the fixed and fair/adaptive PA schemes.

In Figs. 4-7, we study each system impairment (*i.e.*, RTHI, imperfect CSI/SIC) and interference separately from the rest to quantify their effect on the ergodic capacity of the considered NOMA-based system given a fixed PA method between NOMA users.

Fig. 4 aims to analyze the RTHI level impact on the ergodic capacity for U_1/U_2 given $\kappa_i = \{0, 0.1, 0.2\}$. At low and medium SNR values (up to 37 dB), U_1 and U_2 result in similar ergodic capacity values. However, when SNR values rise above 37 dB, the ergodic capacities become sensitive to RTHI. It appears that U_2 is more susceptible to higher κ_i values. On the one hand, the ergodic capacity degradation from the perfect hardware case to $\kappa_i = 0.1$ case is 23% and $\kappa_i = 0.2$ is 49.48%, accordingly, at SNR = 50 dB for U_2. On the other hand, the ergodic capacity diminishes for ideal hardware at $\kappa_i = 0.1$ to 6.575% and at $\kappa_i = 0.2$ to 8.44% for U_1 given SNR = 50 dB. Due to the proportionality of the RTHI level to transmit power and the fact that the power level of U_2 is higher than U_1, the RTHI level has more effect on U_2. In Fig. 4, we also plot the asymptotic ergodic capacity results when the transmit SNR approaches infinity, *i.e.*, high-SNR approximation. In this case, RTHI creates an ergodic capacity ceiling. For instance, when $\kappa_i = 0.1$, U_1 is bounded by 2.3 bits/s/Hz and U_2 by 4.4 bits/s/Hz, correspondingly.

In Fig. 5, we present the ergodic capacity performance versus transmit SNR for different imperfect CSI variance values, $\sigma^2_{ei} = \{0, 005, 0.01, 0.05\}$. Both U_1/U_2 operate at similar ergodic capacity rates when the transmit SNR is below 40 dB. However, it is observed that U_2 is more influenced

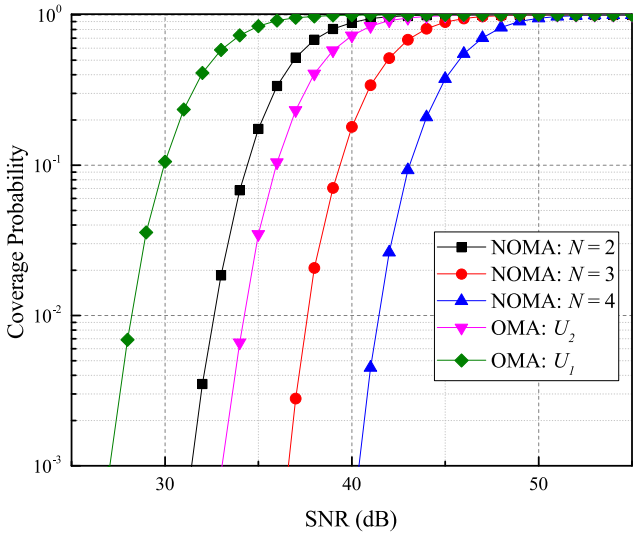

FIGURE 12. Coverage probability versus the transmit SNR at $\xi_i = 0$, $\kappa_i = 0$, $\sigma^2_{ei} = 0$, $M = 24$ for NOMA $N = \{2, 3, 4\}$ and OMA $N = 2$ scenarios.

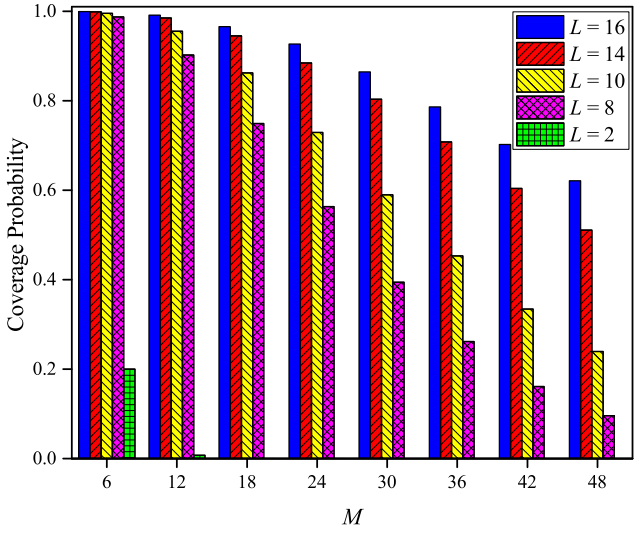

FIGURE 13. Coverage probability versus the number of interferers per cluster, M, for the two-user NOMA network, when $\xi_i = 0$, $\kappa_i = 0$, $\sigma^2_{ei} = 0$, and $L = \{2, 8, 10, 14, 16\}$.

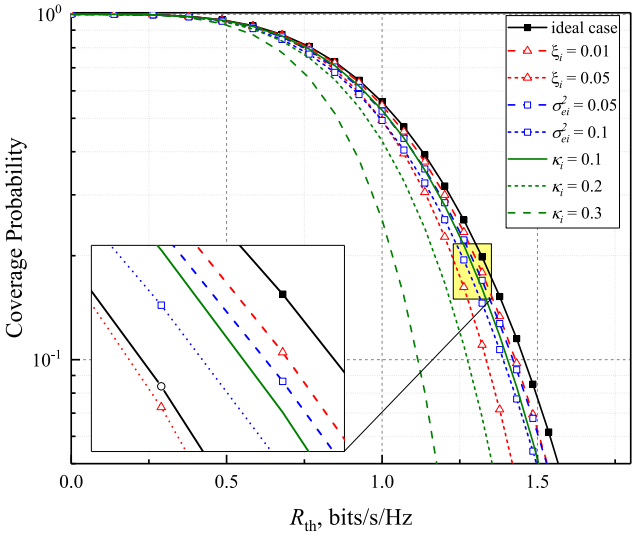

FIGURE 14. Coverage probability versus the rate threshold for the two-user NOMA network at the transmit SNR of 40 dB with $M = 24$ and various system impairments.

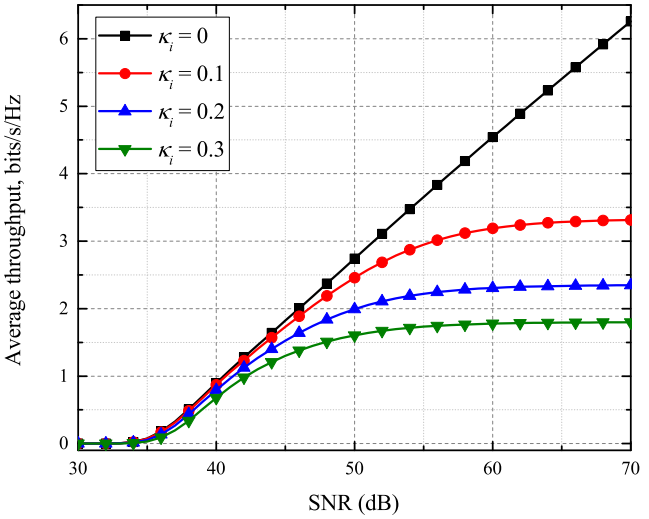

FIGURE 15. Average throughput at $\xi_i = 0$, $\sigma^2_{ei} = 0$, $M = 24$, and $\kappa_i = \{0, 0.1, 0.2, 0.3\}$ for the two-user NOMA network.

by erroneous CSI as opposed to U_1. This matter can also explained by the proportionality of CSI error to the transmit power of U_2 as it was studied above in the discussion of Fig. 4. One can observe that the erroneous CSI starts deteriorating the performance of U_2 for the transmit SNR above 55 dB. Even a small growth of the error variance, *i.e.*, from the ideal case to $\sigma^2_{ei} = 0.005$, bounds the normalized ergodic capacity at 7.3 bits/s/Hz, whereas at the ideal CSI case for SNR = 75 dB the ergodic capacity reaches to 11.7 bits/s/Hz. Likewise, the ergodic capacity is bounded at 6.1 bits/s/Hz for $\sigma^2_{ei} = 0.01$. In addition, considering the performance of U_1, there is ∼0.8 bits/s/Hz difference between the ideal CSI and erroneous CSI plots when the transmit SNR is above 50 dB.

In Fig. 6, we study the impact of imperfect SIC on the performance of U_2. Therefore, the SIC factor varies as $\xi_i = \{0, 0.005, 0.01, 0.05\}$ while the other parameters are set as $\kappa_i = 0$, $\sigma^2_{ei} = 0$, $M = 24$. When the transmit SNR is below 40 dB, there is no obvious evidence of the negative effect of imperfect SIC on the ergodic capacity performance. However, when the SNR goes beyond 40 dB, a detrimental effect of imperfect SIC becomes apparent and puts the following ergodic capacity bounds: $\xi_i = \{0.005, 0.01, 0.05\}$ correspond to the capacity ceilings given by {5.67, 4.7, 2.59} bits/s/Hz, respectively. Considering the ideal SIC case with 11.74 bits/s/Hz achievable at 75 dB, one can draw the following conclusions: $\xi_i = 0.005$ plot shows 2 times,

$\xi_i = 0.01$ plot demonstrates 2.5 times, and $\xi_i = 0.05$ plot results in 4.55 times performance degradation. This figure clearly shows that the error SIC has a significant impact on the normalized ergodic capacity.

In Fig. 7, we vary the number of interfering nodes as $M = \{0, 12, 24, 48\}$ and set $\xi_i = 0$, $\kappa_i = 0$, and $\sigma_{ei}^2 = 0$. From this figure, U_2 notably outperforms U_1. Moreover, the increasing number of interfering nodes significantly degrades the ergodic capacity performance of U_2 at all SNR regions as opposed to the ''no interference'' case. When SNR is above 18 dB, the curve of $M = 0$ plot is higher at least to 6 bits/s/Hz in comparison to $M = \{12, 24, 48\}$ case. Moreover, U_1 is saturated at 2.3 bits/s/Hz even in the ''no interference'' case due to the interference from U_2. From this figure, one can note that interference is a crucial capacity limitation factor in the NOMA-based mmWave D2D mmWawe networks.

In Fig. 8, we plot the normalized ergodic capacity versus the PA coefficient, α_1, for U_1/U_2 at the transmit SNR values of 30, 40 and 50 dB and $\xi_i = 0$, $\kappa_i = 0$, $\sigma_{ei}^2 = 0$, $M = 24$. From this figure, one can notice that the higher α_1 values increase the normalized ergodic capacity of U_1, as opposed to U_2 that experiences the capacity degradation. Intersection points between U_1/U_2 curves represent a fair value for α_1. More precisely, at 30 dB, fair PA coefficients are given by $\alpha_1 = 0.8$ and $\alpha_2 = 0.2$. Similarly, the transmit SNRs of 40 dB and 50 dB correspond to the allocation coefficients $\alpha_1 = 0.84$; $\alpha_2 = 0.16$ and $\alpha_1 = 0.91$; $\alpha_2 = 0.09$, respectively. Therefore, it becomes obvious that the PA scheme needs adaptiveness to maintain some fairness among the users.

B. ADAPTIVE POWER ALLOCATION

In Figs. 9-15, we investigate the ergodic capacity under an optimal fairness-based PA scheme (please refer to Section VI) over all the SNR regions. Our goal is to compare the normalized ergodic capacity of NOMA users at the fair (optimal) and fixed (non-optimal) PA coefficients. If the fairness-based PA coefficients, α_i, are adjusted based on the received powers of U_1 and U_2, the fixed PA coefficients are set as $\alpha_1 = 0.8$ and $\alpha_2 = 0.2$.

In Fig. 9, we set $\xi_i = 0$, $\sigma_{ei}^2 = 0$, $M = 24$ and vary $\kappa_i = \{0.05, 0.16, 0.25\}$ for both fair and fixed PA schemes. From this figure, one can witness the lack of fairness in resource allocation for U_1/U_2 in the fixed PA scheme, which leads to a considerable difference in their performance. For instance, U_2 grows as SNR increases at $\kappa_i = 0.05$ and U_1 plots start saturating above 55 dB for $\kappa_i = \{0.05, 0.16, 0.25\}$ near $2 - 2.25$ bits/s/Hz. However, when the distortion noise level increases to $\kappa_i = 0.16$ for U_2, the ergodic capacity saturates around 3.2 bits/s/Hz. Similarly, we notice that U_2 saturates at 2 bits/s/Hz for $\kappa_i = 0.25$. When the fair PA scheme is applied, both users obtain the similar capacity performance, *i.e.*, $\{4.3, 2.7, 2.1\}$ bits/s/Hz, in the high-SNR regime for $\kappa_i = \{0.05, 0.16, 0.25\}$, respectively. Both fair and fixed PA schemes obtain very similar normalized ergodic capacity sum-rate performances.

In Fig. 10, the individual normalized ergodic capacity is under study at $\xi_i = 0$, $\kappa_i = 0$, $M = 24$, and $\sigma_{ei}^2 = \{0.001, 0.05, 0.1\}$ for both fair and fixed PA schemes. As seen from this figure, the fair PA scheme provides even ergodic capacity performance for U_1/U_2 as opposed to the fixed scheme. For example, when transmit SNR $=$ 55 dB, the corresponding ergodic capacities for U_1 at $\sigma_{ei}^2 = \{0.001, 0.05, 0.1\}$ are recorded as $\{2.17, 2.1, 2.03\}$ bits/s/Hz and for U_2 are $\{5.08, 3.46, 2.79\}$ bits/s/Hz. The fair PA scheme supports the ergodic capacities at the transmit SNR $=$ 55 dB equal to 3.62, 2.85 and 2.49 bits/s/Hz for $\sigma_{ei}^2 = \{0.001, 0.05, 0.1\}$, respectively.

In Fig. 11, we investigate how the LOS/NLOS fading parameters with corresponding PLE values influence on the normalized ergodic capacity of the system with $\xi_i = 0$, $\kappa_i = 0$, $\sigma_{ei}^2 = 0$, $M = 24$ given $m_i = \{2, 4\}$ and $\tau = \{2, 3, 4\}$. Similar to [3], [53], we consider $m_i = 4$ and $\tau = 2$ for the LOS links and $m_i = 2$ and $\tau = \{3, 4\}$ for the NLOS links. As expected, the LOS parameters play a crucial role in the ergodic capacity performance for both fixed and fair PA schemes, especially at low and medium SNR regions. The worst performance was achieved in the NLOS plots with $m_i = 2$ and $\tau = 4$, even a unit difference in PLE made a substantial distinction in the ergodic capacity in comparison to the case with $m_i = 2$ and $\tau = 3$. For instance, for U_2, the $\tau = 3$ plot reaches 2.5 bits/s/Hz at 60 dB, whereas the $\tau = 2$ plot attains 0.1332 bits/s/Hz. Similarly, the $\tau = 3$ and $\tau = 2$ plots achieve 5.625 bits/s/Hz and 0.976 bits/s/Hz at 70 dB, respectively. Moreover, for U_2, the LOS plot with $m_i = 4$ and $\tau = 2$ outperforms the NLOS with $m_i = 2$ and $\tau = 4$ for $\sim$4 bits/s/Hz. In addition, both fair and fixed PA schemes show similar poor performance under the NLOS conditions, when $m_i = 2$ and $\tau = 4$.

In Fig. 12, we investigate the coverage probability versus the transmit SNR for the multi-user NOMA network with $N = \{2, 3, 4\}$ users that apply the fair PA scheme and two-user OMA network given $\xi_i = 0$, $\sigma_{ei}^2 = 0$, $\kappa_i = 0$, and $M = 24$. When $P_c^{[i]} = 0.1$, there is a 5 dB performance degradation from the NOMA $N = 3$ to $N = 2$ case, and similarly, there is 3.7 dB drop from the NOMA $N = 3$ to $N = 4$ scenario. It is imperative to note that a two-user NOMA network has shown the advantage over the three-/four-user NOMA network. From this figure, OMA U_1 shows a higher coverage probability performance than the optimized NOMA U_i. However, optimized NOMA U_i performs better than the OMA U_2.

In Fig. 13, we studied the coverage probability versus number of i.n.i.d. interfering nodes, $M = \{6 : 6 : 48\}$, for different numbers of antenna elements per device node, $L = \{2, 8, 10, 14, 16\}$, at the transmit $SNR = 40$ dB, $\xi_i = 0$, $\sigma_{ei}^2 = 0$, $\kappa_i = 0$, and $N = 2$. This figure showcases the essence of the number of interfering nodes on the performance of the coverage probability. There is an alternating slope of change in the coverage probability plots due to the alternating antenna gain factors of $G_s \times G_s$ and $G_m \times G_s$. Moreover, this figure justifies that a higher number of antenna

elements per device node tackles the problem of interference since a higher number of antenna elements increases antenna gain and suppresses the side/back lobe antenna gains. From $L = 2$ to $L = 16$, a network from being at the idle state above $M = 6$ shows the lowest coverage probability performance of 0.6 at $M = 48$.

In Fig. 14, we analyze how the imperfect SIC/CSI level deteriorate the coverage probability versus the rate threshold, R_{th}, given $\xi_i = \{0, 0.01, 0.05\}$, $\kappa_i = \{0, 0.1, 0.2, 0.3\}$, $\sigma_{ei}^2 = \{0, 0.05, 0.1\}$, $M = 24$ and transmit SNR of 40 dB. For the low rate requirements (up to 0.5 bits/s/Hz), the system obtains the same performance irrespective of the amount and type of considered impairments. However, at higher rate thresholds, one can observe that the coverage metric degrades fast and non-linearly (even for the ideal case) as R_{th} increases. For instance, for the rate thresholds given by $R_{th} = \{0.6, 0.8, 1\}$ bits/s/Hz, the system with ideal settings achieves the coverage probability of $P_c^{[i]} = \{0.8, 0.75, 0.56\}$, accordingly. Moreover, it is noted that the hardware imperfections have the most significant impact on the coverage metric. Imperfect SIC has less influence on the coverage probability. At the same time, it is apparent that the considered system model is more robust to the imperfect CSI compared to the other impairments.

Finally, in Fig. 15, we study the average throughput performance versus the transmit SNR given $\xi_i = 0$, $\sigma_{ei}^2 = 0$, $M = 24$, and $\kappa_i = \{0, 0.1, 0.2, 0.3\}$ for the two-user NOMA network. From this figure, we notice that the RTHI level greatly influences the average throughput that causes performance saturation at the SNR above 40 dB. Below 40 dB all the plots demonstrate similar average throughput performance. For instance, a plot with $\kappa_i = 0.1$ saturates at average throughput, 3.4 bits/s/Hz, $\kappa_i = 0.2$ saturates at 2.4 bits/s/Hz, and $\kappa_i = 0.3$ saturates at 1.8 bits/s/Hz. In the mid-SNR region (at 55 dB), the ideal case results in 3.65 bits/s/Hz, $\kappa_i = 0.1$ at 2.96 bits/s/Hz, $\kappa_i = 0.2$ at 2.96 bits/s/Hz, and $\kappa_i = 0.3$ at 1.7 bits/s/Hz of average throughput, correspondingly. Hence, there is a twice performance degradation from the ideal case to the $\kappa_i = 0.3$ case. This figure justifies the significance of the RTHI impact on the high-rate systems.

VIII. CONCLUSION

In this work, we have studied the integrated model of 5G technologies as D2D communication and NOMA operating on mmWave frequencies by considering practical system limitations such as RTHI, imperfect CSI/SIC, and i.n.i.d. interference noises. These system imperfections inevitably limit the ergodic capacity performance of future communication systems; especially, interference has a strong influence on the ergodic capacity. Interference can be combated by increasing the number of antenna elements per device node, introducing additional costs to the network. The simulation results of this work carefully investigated each system impairment separately and proved the importance of practical system settings. We obtained mathematically tractable ergodic capacity formulas with their tight upper and lower bounds as well as asymptotic ergodic capacity expressions that provide valuable insights into the effect of each system impairment. Moreover, we have derived comprehensive coverage probability and average throughput formulas that enable further performance analysis of the proposed system model. The user-fairness-based PA scheme presented in this work provides a fair resource allocation for all NOMA users.

APPENDIX A
DERIVATION OF THE ERGODIC CAPACITY

The closed-form expression for ergodic capacity in (12) is evaluated by using (11) and (7), as shown in (A.1), at the bottom of the page. Since $T^{[i]}$ is the summation of $X^{[i]}(a_j^{[i]} + b_j^{[i]})$ and $Z^{[i]}$ RVs, we first approximate the fading and scale parameters of $Z^{[i]}$ RV, which represents a summation of M i.n.i.d. interfering nodes. With this in mind, we define $Z^{[i]} \sim Gamma(\tilde{m}_t, \tilde{\beta}_t)$, where $\tilde{m}$ and $\tilde{\beta}$ are evaluated as given in Lemma 1. Similarly, the second round of approximation is applied to find the fading and scale parameters for $T^{[i]}$ as $T^{[i]} \sim Gamma(\hat{m}_t, \hat{\beta}_t)$. Next, we rewrite the $\mathbb{E}\{\ln\left(1 + \frac{t}{\Lambda^{[i]}}\right)\}$ term with the aid of Meijer G-function as $\ln\left(1 + \frac{t}{\Lambda^{[i]}}\right) = G_{2,2}^{1,2}\left(\frac{t}{\Lambda^{[i]}}\middle|\begin{smallmatrix}1,1\\1,0\end{smallmatrix}\right)$ from [69, (8.4.6.5)] and evaluate the integral A_1 by using [52, (7.813.1)] as

$$A_1 = \int_0^{\infty} \frac{t^{\hat{m}_t - 1} \exp\left(-\frac{t}{\hat{\beta}_t}\right)}{\ln(2)\,\Gamma\left(\hat{m}_t\right)\hat{\beta}_t^{\hat{m}_t}} G_{2,2}^{1,2}\left(\frac{t}{\Lambda^{[i]}}\middle|\begin{smallmatrix}1,1\\1,0\end{smallmatrix}\right) \mathrm{d}t = \frac{G_{3,2}^{1,3}\left(\frac{\hat{\beta}_t}{\Lambda^{[i]}}\middle|\begin{smallmatrix}1-\hat{m}_t,1,1\\1,0\end{smallmatrix}\right)}{\ln(2)\,\Gamma\left(\hat{m}_t\right)}. \tag{A.2}$$

Similarly, $V^{[i]}$ is the summation of $b_j^{[i]}X^{[i]}$ and $Z^{[i]}$ RVs. A single gamma approximation for $T^{[i]}$ RV is approximated

$$C_j^{[i]} = \mathbb{E}\left\{\log_2\left(\Lambda^{[i]} + T^{[i]}\right)\right\} - \mathbb{E}\left\{\log_2\left(\Lambda^{[i]} + V^{[i]}\right)\right\} = \mathbb{E}\left\{\log_2\left(\Lambda^{[i]}\left(1 + \frac{T^{[i]}}{\Lambda^{[i]}}\right)\right)\right\}$$
$$- \mathbb{E}\left\{\log_2\left(\Lambda^{[i]}\left(1 + \frac{V^{[i]}}{\Lambda^{[i]}}\right)\right)\right\} = \underbrace{\int_0^{\infty} \log_2\left(1 + \frac{t}{\Lambda^{[i]}}\right) f_{T^{[i]}}(t)\mathrm{d}t}_{A_1} - \underbrace{\int_0^{\infty} \log_2\left(1 + \frac{v}{\Lambda^{[i]}}\right) f_{V^{[i]}}(v)\mathrm{d}v}_{A_2} \tag{A.1}$$

by $V^{[i]} \sim Gamma(\hat{m}_v, \hat{\beta}_v)$ and evaluated as

$$A_2 = \int_0^\infty \frac{v^{\hat{m}_v - 1} \exp\left(-\frac{v}{\hat{\beta}_v}\right)}{\ln_2 \Gamma(\hat{m}_v)\hat{\beta}_v^{\hat{m}_v}} G_{2,2}^{1,2}\left(\frac{v}{\Lambda^{[i]}} \middle| \begin{matrix} 1,1 \\ 1,0 \end{matrix}\right) \mathrm{d}v$$
$$= \frac{G_{3,2}^{1,3}\left(\frac{\hat{\beta}_v}{\Lambda^{[i]}} \middle| \begin{matrix} 1-\hat{m}_v, 1, 1 \\ 1, 0 \end{matrix}\right)}{\ln(2)\Gamma(\hat{m}_v)}. \quad \text{(A.3)}$$

Now, by using (22) and (23), we obtain the ergodic capacity formula in (12).

APPENDIX B
DERIVATION OF THE LOWER ERGODIC CAPACITY

To compute the lower ergodic capacity, it is essential to find the expressions $\mathbb{E}\{\ln(a_j^{[i]} X^{[i]})\}$ and $\mathbb{E}\{\ln(\Lambda^{[i]} + V^{[i]})\}$. The first term is obtained with the aid of [52, (4.352.1)] and the PDF of Nakagami-m fading with m_i fading and β_i scale parameters [61, (5.14)] as

$$\mathbb{E}\{\ln\left(a_j^{[i]} X^{[i]}\right)\} = \ln\left(a_j^{[i]}\right) + \int_0^\infty \ln(x) f_{X^{[i]}}(x)\, \mathrm{d}x$$
$$= \ln\left(a_j^{[i]}\right) + \frac{1}{\Gamma(m_i)\beta_i^{m_i}} \int_0^\infty x^{m_i - 1} \times \exp\left(-\frac{x}{\beta_i}\right) \ln(x)\, \mathrm{d}x$$
$$= \ln\left(a_j^{[i]} \beta_i\right) + \psi(m_i). \quad \text{(B.1)}$$

Moreover, $\mathbb{E}\{\ln\left(\Lambda^{[i]} + V^{[i]}\right)\}$ is evaluated similarly to (B.1). Hence, the final expression for the lower ergodic capacity is displayed in (13).

APPENDIX C
DERIVATION OF THE UPPER ERGODIC CAPACITY

Key components to evaluate the upper ergodic capacity analysis are $\mathbb{E}\{X^{[i]}\}$ and $\mathbb{E}\left(1/\left(\Lambda^{[i]} + V^{[i]}\right)\right)$. We begin with the calculation of $\mathbb{E}\{X^{[i]}\}$ below

$$\mathbb{E}\{X^{[i]}\} = \int_0^\infty x \frac{x^{m_i - 1} \exp(-\frac{x}{\beta_i})}{\Gamma(m_i)\beta_i^{m_i}} \mathrm{d}x$$
$$= \frac{\beta_i \Gamma(1 + m_i)}{\Gamma(m_i)} = \beta_i m_i. \quad \text{(C.1)}$$

Next, we evaluate the second component as

$$\mathbb{E}\left\{\frac{1}{\Lambda^{[i]} + V^{[i]}}\right\} = \int_0^\infty \frac{v^{\hat{m}_v - 1} \exp\left(-\frac{v}{\hat{\beta}_v}\right)}{\Gamma(\hat{m}_v)\hat{\beta}_v^{\hat{m}_v}\left(v + \Lambda^{[i]}\right)} \mathrm{d}v$$
$$= \frac{\Lambda^{[i]-1+\hat{m}_v}}{\hat{\beta}_v^{\hat{m}_v}} \exp\left(\frac{\Lambda^{[i]}}{\hat{\beta}_v}\right) \Gamma \times \left(1 - \hat{m}_v, \frac{\Lambda^{[i]}}{\hat{\beta}_v}\right). \quad \text{(C.2)}$$

By applying (C.1) and (C.2) into (10), we obtain the expression for the upper ergodic capacity in (14).

APPENDIX D
DERIVATION OF THE ASYMPTOTIC ERGODIC CAPACITY AT HIGH-SNR REGIME

To evaluate the asymptotic ergodic capacity formula at high-SNR, regime the SINDR formula in (3) is revisited. Next, by using the definition of transmit SNR, $\mathrm{SNR}_i = \frac{\rho_i}{\sigma_i^2}$, one can rewrite the SINDR in terms of SNR as

$$\gamma_j^{[i]} = \frac{\alpha_j \mathrm{SNR}_i X^{[i]}}{\mathcal{B}_j \mathrm{SNR}_i X^{[i]} + 1 + \mathrm{SNR}_i(1 + \kappa_i^2)\sigma_{ei}^2 + \frac{\eta}{\sigma_i^2}}, \quad \text{(D.1)}$$

where $X^{[i]} = |\tilde{h}_i|^2$ and η represents the interference term as $\eta = \sum_{k=1}^{M} |g_{ik}|^2 \left(1 + \bar{\kappa}_k^2\right) \bar{\rho}_{ik}$. Now, let us divide both the numerical and denominator parts in (D.1) by SNR_i to obtain the simplified representation of the SINDR as

$$\gamma_j^{[i]} = \frac{\alpha_j X^{[i]}}{\mathcal{B}_j X^{[i]} + \frac{1}{\mathrm{SNR}_i} + (1 + \kappa_i^2)\sigma_{ei}^2 + \frac{\eta}{\sigma_i^2 \mathrm{SNR}_i}}, \quad \text{(D.2)}$$

First, we find the SINDR at high-SNR regime by taking the limit of SINDR in (D.2), when SNR tends to infinity as

$$\tilde{\gamma}_j^{[i]} = \lim_{\mathrm{SNR}_i \to \infty} \gamma_j^{[i]} = \frac{\alpha_j X^{[i]}}{\mathcal{B}_j X^{[i]} + (1 + \kappa_i^2)\sigma_{ei}^2}. \quad \text{(D.3)}$$

By applying the high-SNR approximated SINDR in (D.3) and by using Jensen's inequality, we derive the asymptotic ergodic capacity as

$$\tilde{C}_j^{[i]} = \mathbb{E}\{\log_2(1 + \tilde{\gamma}_j^{[i]})\} = \log_2\left(1 + \mathbb{E}\{\tilde{\gamma}_j^{[i]}\}\right)$$
$$= \log_2\left(1 + \frac{\mathbb{E}\{\alpha_j X^{[i]}\}}{\underbrace{\mathbb{E}\{\mathcal{B}_j X^{[i]} + (1 + \kappa_i^2)\sigma_{ei}^2\}}_{\Xi}}\right). \quad \text{(D.4)}$$

The evaluation of the denominator Ξ in (D.4) is given as

$$\mathbb{E}\{\mathcal{B}_j X^{[i]} + (1 + \kappa_i^2)\sigma_{ei}^2\}$$
$$= \int_0^\infty \left(\mathcal{B}_j x + \left(1 + \kappa_i^2\right)\sigma_{ei}^2\right) x^{m_i - 1} \exp\left(-\frac{x}{\beta_i}\right) \mathrm{d}x$$
$$= \left(1 + \kappa_i^2\right)\sigma_{ei}^2 + \mathcal{B}_j \beta_i m_i. \quad \text{(D.5)}$$

Derivation of the numerator part Ξ is obtained identically to (C.1) and written as $\mathbb{E}\{\alpha_j X^{[i]}\} = \alpha_j \beta_i m_i$. Hence, we present the final asymptotic ergodic capacity (*i.e.,* capacity ceiling) in (15).

APPENDIX E
DERIVATION OF THE COVERAGE PROBABILITY

The proof of *Proposition 4* that presents the coverage probability for the proposed system model is calculated below

$$P_{\mathrm{c}}^{[i]}(v) = \Pr\left(\frac{a_j^{[i]} X^{[i]}}{b_i^{[j]} X^{[i]} + Z + \Lambda^{[i]}} > v\right)$$

$$= \int_0^{\infty} \left(1 - F_{X^{[i]}}\left(\frac{v(\Lambda^{[i]}+z)}{a_j^{[i]} - v b_j^{[i]}}\right)\right) f_z(z)\mathrm{d}z, \quad \text{(E.1)}$$

when $0 \leq v < \frac{a_j^{[i]}}{b_j^{[i]}}$; otherwise, it equals to 0. The CDF of $X^{[i]}$ Gamma RV is given in (20).

Now, (E.1) can be evaluated as

$$P_{\mathrm{c}}^{[i]}(v) = \int_0^{\infty} \exp\left(-\omega_i\left(\Lambda^{[i]}+z\right) \sum_{t=0}^{m_i-1} \frac{\left(\omega_i\left(\Lambda^{[i]}+z\right)\right)^t}{t!}\right) \times z^{\tilde{m}_t-1} \exp\left(-\frac{z}{\tilde{\beta}_t}\right) \mathrm{d}z \times \frac{1}{\Gamma(\tilde{m}_t)\tilde{\beta}_t^{\tilde{m}_t}}. \quad \text{(E.2)}$$

Let us assign $\omega_i = \frac{v}{\beta_i(a_j^{[i]} - v b_j^{[i]})}$ for simplicity. With the aid of the power of binomials [52, (1.111)], we expand $\left(\omega_i\left(\Lambda^{[i]}+z\right)\right)^t = \omega_i^t \sum_{k=0}^{t} \binom{t}{k} \Lambda^{[i]t-k} z^k$. Now, by placing the expanded term into (E.2), we obtain

$$P_{\mathrm{c}}^{[i]}(v) = \frac{1}{\Gamma(\tilde{m}_t)\tilde{\beta}_t^{\tilde{m}_t}} \sum_{t=0}^{m_i-1} \frac{\omega_i^t}{t!} \sum_{k=0}^{t} \binom{t}{k} \Lambda^{[i]t-k} \times \int_0^{\infty} z^{k+\tilde{m}_t-1} \exp\left(-\omega_i(\Lambda^{[i]}+z) - \frac{z}{\tilde{\beta}_w}\right) \mathrm{d}z. \quad \text{(E.3)}$$

The integral in (E.3) is evaluated by using [52, (8.310.1)] and the closed-form expression for the coverage probability is obtained in (18).

REFERENCES

[1] (2020). *5G–Fifth Generation of Mobile Technologies*. Accessed: Aug. 18, 2020. [Online]. Available: https://www.itu.int/en/mediacentre/backgrounders/Pages/5G-fifth-generation-of-mobile-technologies.aspx

[2] R. I. Ansari, "5G D2D networks: Techniques, challenges, and future prospects," *IEEE Syst. J.*, vol. 12, no. 4, pp. 3970–3984, Dec. 2018.

[3] K. Venugopal, M. C. Valenti, and R. W. Heath, Jr., "Device-to-device millimeter wave communications: Interference, coverage, rate, and finite topologies," *IEEE Trans. Wireless Commun.*, vol. 15, no. 9, pp. 6175–6188, Sep. 2016.

[4] J. Zhao, Y. Liu, K. K. Chai, Y. Chen, M. Elkashlan, and J. Alonso-Zarate, "NOMA-based D2D communications: Towards 5G," in *Proc. IEEE Global Commun. Conf. (GLOBECOM)*, Washington, DC, USA, Dec. 2016, pp. 1–6.

[5] A. N. Uwaechia and N. M. Mahyuddin, "A comprehensive survey on millimeter wave communications for fifth-generation wireless networks: Feasibility and challenges," *IEEE Access*, vol. 8, pp. 62367–62414, 2020.

[6] J. G. Andrews, T. Bai, M. N. Kulkarni, A. Alkhateeb, A. K. Gupta, and R. W. Heath, Jr., "Modeling and analyzing millimeter wave cellular systems," *IEEE Trans. Commun.*, vol. 65, no. 1, pp. 403–430, Jan. 2017.

[7] Z. Ding, P. Fan, and H. V. Poor, "Random beamforming in millimeter-wave NOMA networks," *IEEE Access*, vol. 5, pp. 7667–7681, 2017.

[8] S. Rangan, T. S. Rappaport, and E. Erkip, "Millimeter-wave cellular wireless networks: Potentials and challenges," *Proc. IEEE*, vol. 102, no. 3, pp. 366–385, Mar. 2014.

[9] Z. Ding, X. Lei, G. K. Karagiannidis, R. Schober, J. Yuan, and V. Bhargava, "A survey on non-orthogonal multiple access for 5G networks: Research challenges and future trends," *IEEE J. Sel. Areas Commun.*, vol. 35, no. 10, pp. 2181–2195, Oct. 2017.

[10] S. M. R. Islam, N. Avazov, O. A. Dobre, and K.-S. Kwak, "Power-domain non-orthogonal multiple access (NOMA) in 5G systems: Potentials and challenges," *IEEE Commun. Surveys Tuts.*, vol. 19, no. 2, pp. 721–742, 2nd Quart., 2017.

[11] S. Arzykulov, G. Nauryzbayev, M. S. Hashmi, A. M. Eltawil, K. M. Rabie, and S. Seilov, "Hardware- and interference-limited cognitive IoT relaying NOMA networks with imperfect SIC over generalized non-homogeneous fading channels," *IEEE Access*, vol. 8, pp. 72942–72956, 2020.

[12] G. Nauryzbayev, M. Abdallah, and H. Elgala, "On the performance of NOMA-enabled spectrally and energy efficient OFDM (SEE-OFDM) for indoor visible light communications," in *Proc. IEEE 87th Veh. Technol. Conf. (VTC Spring)*, Porto, Portugal, Jun. 2018, pp. 1–5.

[13] S. Arzykulov, G. Nauryzbayev, A. Celik, and A. M. Eltawil, "Hardware and interference limited cooperative CR-NOMA networks under imperfect SIC and CSI," *IEEE Open J. Commun. Soc.*, vol. 2, pp. 1473–1485, 2021.

[14] G. Nauryzbayev, M. Abdallah, and H. Elgala, "Outage of SEE-OFDM VLC-NOMA networks," *IEEE Photon. Technol. Lett.*, vol. 31, no. 2, pp. 121–124, Jan. 15, 2019.

[15] A. Benjebbour, Y. Kishiyama, and Y. Okumura, "Field trials of improving spectral efficiency by using a smartphone-sized NOMA chipset," *NTT DOCOMO Tech. J.*, vol. 20, no. 1, pp. 4–13, Jul. 2018.

[16] G. Nauryzbayev, E. Alsusa, and M. Abdallah, "On the feasibility of interference alignment in compounded MIMO broadcast channels with antenna correlation and mixed user classes," *IEEE Trans. Veh. Technol.*, vol. 67, no. 3, pp. 2130–2140, Mar. 2018.

[17] S. M. A. Kazmi, N. H. Tran, T. M. Ho, A. Manzoor, D. Niyato, and C. S. Hong, "Coordinated device-to-device communication with non-orthogonal multiple access in future wireless cellular networks," *IEEE Access*, vol. 6, pp. 39860–39875, 2018.

[18] Y. Dai, M. Sheng, J. Liu, N. Cheng, X. Shen, and Q. Yang, "Joint mode selection and resource allocation for D2D-enabled NOMA cellular networks," *IEEE Trans. Veh. Technol.*, vol. 68, no. 7, pp. 6721–6733, Jul. 2019.

[19] J.-B. Kim, I.-H. Lee, and J.-H. Lee, "Capacity scaling for D2D aided cooperative relaying systems using NOMA," *IEEE Commun. Lett.*, vol. 7, no. 1, pp. 42–45, Feb. 2018.

[20] R. Méndez-Rial, C. Rusu, N. González-Prelcic, A. Alkhateeb, and R. W. Heath, Jr., "Hybrid MIMO architectures for millimeter wave communications: Phase shifters or switches?" *IEEE Access*, vol. 4, pp. 247–267, 2016.

[21] M. U. Aminu, J. Lehtomaki, and M. Juntti, "Beamforming and transceiver optimization with phase noise for mmWave and THz bands," in *Proc. 16th Int. Symp. Wireless Commun. Syst. (ISWCS)*, Oulu, Finland, Aug. 2019, pp. 1–5.

[22] Z. Chen and F. F. Dai, "Effects of LO phase and amplitude imbalances and phase noise on M-QAM transceiver performance," *IEEE Trans. Ind. Electron.*, vol. 57, no. 5, pp. 1505–1517, May 2010.

[23] M. Majidi, A. Mohammadi, and A. Abdipour, "Analysis of the power amplifier nonlinearity on the power allocation in cognitive radio networks," *IEEE Trans. Commun.*, vol. 62, no. 2, pp. 467–477, Feb. 2014.

[24] B. Selim, S. Muhaidat, P. C. Sofotasios, B. S. Sharif, and T. Stouraitis, "Performance analysis of non-orthogonal multiple access under I/Q imbalance," *IEEE Access*, vol. 6, pp. 18453–18468, 2018.

[25] R. Maršálek, M. Pospíšil, T. Gotthans, and T. Urbanec, "60 GHz setup for RF components impairments compensation," in *IEEE MTT-S Int. Microw. Symp. Dig.*, Dublin, Ireland, Aug. 2018, pp. 1–3.

[26] L. Tlebaldiyeva and T. Tsiftsis, "Underlay cognitive radio with imperfect transceiver electronics under Nakagami-m fading," in *Proc. Int. Conf. Comput. Netw. Commun. (CoCoNet)*, Astana, Kazakhstan, Aug. 2018, pp. 58–63.

[27] T. Schenk, *RF Imperfections in High-Rate Wireless Systems: Impact and Digital Compensation*. Dordrecht, The Netherlands: Springer, 2008.

[28] R. Gomes, L. Sismeiro, C. Ribeiro, T. R. Fernandes, M. G. Sanchez, A. Hammoudeh, and R. F. S. Caldeirinha, "Will COTS RF front-ends really cope with 5G requirements at mmWave?" *IEEE Access*, vol. 6, pp. 38745–38769, 2018.

[29] E. Björnson, J. Hoydis, M. Kountouris, and M. Debbah, "Massive MIMO systems with non-ideal hardware: Energy efficiency, estimation, and capacity limits," *IEEE Trans. Inf. Theory*, vol. 60, no. 11, pp. 7112–7139, Nov. 2014.

[30] L. Zhu, J. Zhang, Z. Xiao, X. Cao, D. O. Wu, and X.-G. Xia, "Joint power control and beamforming for uplink non-orthogonal multiple access in 5G millimeter-wave communications," *IEEE Trans. Wireless Commun.*, vol. 17, no. 9, pp. 6177–6189, Sep. 2018.

[31] A. Papazafeiropoulos, S. K. Sharma, S. Chatzinotas, and B. Ottersten, "Ergodic capacity analysis of AF DH MIMO relay systems with residual transceiver hardware impairments: Conventional and large system limits," *IEEE Trans. Veh. Technol.*, vol. 66, no. 8, pp. 7010–7025, Aug. 2017.

[32] F. Ding, H. Wang, S. Zhang, and M. Dai, "Impact of residual hardware impairments on non-orthogonal multiple access based amplify-and-forward relaying networks," *IEEE Access*, vol. 6, pp. 15117–15131, 2018.

[33] C. K. Singh, V. Singh, P. K. Upadhyay, and M. Lin, "Energy harvesting in overlay cognitive NOMA systems with hardware impairments," *IEEE Syst. J.*, early access, Jun. 8, 2021, doi: 10.1109/JSYST.2021.3082552.

[34] A. K. Shukla, V. Singh, P. K. Upadhyay, A. Kumar, and J. M. Moualeu, "Performance analysis of energy harvesting-assisted overlay cognitive NOMA systems with incremental relaying," *IEEE Open J. Commun. Soc.*, vol. 2, pp. 1558–1576, 2021.

[35] X. Li, J. Li, Y. Liu, Z. Ding, and A. Nallanathan, "Residual transceiver hardware impairments on cooperative NOMA networks," *IEEE Trans. Wireless Commun.*, vol. 19, no. 1, pp. 680–695, Jan. 2020.

[36] M. Li, B. Selim, S. Muhaidat, P. C. Sofotasios, M. Dianati, P. D. Yoo, J. Liang, and A. Wang, "Effects of residual hardware impairments on secure NOMA-based cooperative systems," *IEEE Access*, vol. 8, pp. 2524–2536, 2020.

[37] K. Belbase, C. Tellambura, and H. Jiang, "Coverage analysis of cooperative NOMA in millimeter wave networks," *IEEE Commun. Lett.*, vol. 23, no. 12, pp. 2154–2158, Dec. 2019.

[38] Y. Gao, B. Xia, Y. Liu, Y. Yao, K. Xiao, and G. Lu, "Analysis of the dynamic ordered decoding for uplink NOMA systems with imperfect CSI," *IEEE Trans. Veh. Technol.*, vol. 67, no. 7, pp. 6647–6651, Jul. 2018.

[39] X. Yan, J. Ge, Y. Zhang, and L. Gou, "NOMA-based multiple-antenna and multiple-relay networks over Nakagami-*m* fading channels with imperfect CSI and SIC error," *IET Commun.*, vol. 12, no. 17, pp. 2087–2098, Oct. 2018.

[40] X. Yan, H. Xiao, K. An, G. Zheng, and S. Chatzinotas, "Ergodic capacity of NOMA-based uplink satellite networks with randomly deployed users," *IEEE Syst. J.*, vol. 14, no. 3, pp. 3343–3350, Sep. 2020.

[41] A. Tregancini, C. H. M. Lima, E. E. B. Olivo, and H. Alves, "Performance analysis framework for NOMA systems over non-identical Nakagami-*m* fading channels," in *Proc. 16th Int. Symp. Wireless Commun. Syst. (ISWCS)*, Oulu, Finland, Aug. 2019, pp. 150–154.

[42] N. I. Miridakis, E. T. Michailidis, A. Michalas, E. Skondras, D. J. Vergados, and D. D. Vergados, "Performance of uplink NOMA with user mobility under short packet transmission," 2021, *arXiv:2108.04677*.

[43] Z. Ding, R. Schober, P. Fan, and H. Vincent Poor, "OTFS-NOMA: An efficient approach for exploiting heterogenous user mobility profiles," *IEEE Trans. Commun.*, vol. 67, no. 11, pp. 7950–7965, Nov. 2019.

[44] D. Darsena, I. Iudice, and F. Verde, "Reception strategies for sky-ground uplink non-orthogonal multiple access," 2021, *arXiv:2108.06713*.

[45] K. S. Ali, H. Elsawy, A. Chaaban, and M.-S. Alouini, "Non-orthogonal multiple access for large-scale 5G networks: Interference aware design," *IEEE Access*, vol. 5, pp. 21204–21216, 2017.

[46] S. Arzykulov, G. Nauryzbayev, T. A. Tsiftsis, B. Maham, M. S. Hashmi, and K. M. Rabie, "Underlay spectrum sharing for NOMA relaying networks: Outage analysis," in *Proc. Int. Conf. Comput., Netw. Commun. (ICNC)*, Big Island, HI, USA, Feb. 2020, pp. 897–901.

[47] C. Studer, M. Wenk, and A. Burg, "MIMO transmission with residual transmit-RF impairments," in *Proc. Int. ITG Workshop Smart Antennas (WSA)*, Feb. 2010, pp. 189–196.

[48] X. Zhang, M. Matthaiou, E. Bjornson, M. Coldrey, and M. Debbah, "On the MIMO capacity with residual transceiver hardware impairments," in *Proc. IEEE Int. Conf. Commun. (ICC)*, Jun. 2014, pp. 5299–5305.

[49] A. Papazafeiropoulos, S. K. Sharma, T. Ratnarajah, and S. Chatzinotas, "Impact of residual additive transceiver hardware impairments on Rayleigh-product MIMO channels with linear receivers: Exact and asymptotic analyses," *IEEE Trans. Commun.*, vol. 66, no. 1, pp. 105–118, Jan. 2018.

[50] O. Taghizadeh, V. Radhakrishnan, A. C. Cirik, R. Mathar, and L. Lampe, "Hardware impairments aware transceiver design for bidirectional full-duplex MIMO OFDM systems," *IEEE Trans. Veh. Technol.*, vol. 67, no. 8, pp. 7450–7464, Aug. 2018.

[51] S. Covo and A. Elalouf, "A novel single-gamma approximation to the sum of independent gamma variables, and a generalization to infinitely divisible distributions," *Electron. J. Statist.*, vol. 8, no. 1, pp. 894–926, Jan. 2014.

[52] I. S. Gradshteyn and I. M. Ryzhik, *Table of Integrals, Series, and Products*, 7th ed. Amsterdam, The Netherlands: Elsevier, 2007.

[53] S. Kusaladharma, Z. Zhang, and C. Tellambura, "Interference and outage analysis of random D2D networks underlaying millimeter-wave cellular networks," *IEEE Trans. Commun.*, vol. 67, no. 1, pp. 778–790, Jan. 2019.

[54] H. Li, Y. D. Yao, and J. Yu, "Outage probabilities of wireless systems with imperfect beamforming," *IEEE Trans. Veh. Technol.*, vol. 55, no. 5, pp. 1503–1515, Sep. 2006.

[55] J. Wildman, P. H. J. Nardelli, M. Latva-Aho, and S. Weber, "On the joint impact of beamwidth and orientation error on throughput in directional wireless Poisson networks," *IEEE Trans. Wireless Commun.*, vol. 13, no. 12, pp. 7072–7085, Dec. 2014.

[56] S. Kusaladharma, W.-P. Zhu, and W. Ajib, "Outage performance and average rate for large-scale millimeter-wave NOMA networks," *IEEE Trans. Wireless Commun.*, vol. 19, no. 2, pp. 1280–1291, Feb. 2020.

[57] T. Bai and R. W. Heath, Jr., "Coverage and rate analysis for millimeter-wave cellular networks," *IEEE Trans. Wireless Commun.*, vol. 14, no. 2, pp. 1100–1114, Feb. 2015.

[58] Z. Ding, H. Dai, and H. V. Poor, "Relay selection for cooperative NOMA," *IEEE Wireless Commun. Lett.*, vol. 5, no. 4, pp. 416–419, Aug. 2016.

[59] A. K. Gupta and J. F. Buckwalter, "Linearity considerations for low-EVM, millimeter-wave direct-conversion modulators," *IEEE Trans. Microw. Theory Techn.*, vol. 60, no. 10, pp. 3272–3285, Oct. 2012.

[60] C. Zhong, M. Matthaiou, G. K. Karagiannidis, and T. Ratnarajah, "Generic ergodic capacity bounds for fixed-gain AF dual-hop relaying systems," *IEEE Trans. Veh. Technol.*, vol. 60, no. 8, pp. 3814–3824, Oct. 2011.

[61] I. S. Ansari, F. Yilmaz, M.-S. Alouini, and O. Kucur, "On the sum of gamma random variates with application to the performance of maximal ratio combining over Nakagami-*m* fading channels," in *Proc. IEEE 13th Int. Workshop Signal Process. Adv. Wireless Commun. (SPAWC)*, Cesme, Turkey, Jun. 2012, pp. 394–398.

[62] P. G. Moschopoulos, "The distribution of the sum of independent Gamma random variables," *Ann. Inst. Statist. Math.*, vol. 37, no. 1, pp. 541–544, 1985.

[63] Y. Akhmetkaziyev, G. Nauryzbayev, S. Arzykulov, A. M. Eltawil, K. M. Rabie, and X. Li, "Performance of NOMA-enabled cognitive satellite-terrestrial networks with non-ideal system limitations," *IEEE Access*, vol. 9, pp. 35932–35946, 2021.

[64] Z. Ding, M. Peng, and H. V. Poor, "Cooperative non-orthogonal multiple access in 5G systems," *IEEE Commun. Lett.*, vol. 19, no. 8, pp. 1462–1465, Aug. 2015.

[65] O. L. A. López, H. Alves, P. H. J. Nardelli, and M. Latva-Aho, "Aggregation and resource scheduling in machine-type communication networks: A stochastic geometry approach," *IEEE Trans. Wireless Commun.*, vol. 17, no. 7, pp. 4750–4765, Jul. 2018.

[66] E. Bjornson, M. Matthaiou, and M. Debbah, "A new look at dual-hop relaying: Performance limits with hardware impairments," *IEEE Trans. Commun.*, vol. 61, no. 11, pp. 4512–4525, Nov. 2013.

[67] X. Liu and J. Mo, "Spectral-energy efficiency maximization for wireless powered low-latency NOMA systems with full-duplex relaying," *EURASIP J. Wireless Commun. Netw.*, vol. 2019, no. 1, p. 206, Dec. 2019.

[68] C. E. Garcia, M. R. Camana, and I. Koo, "Joint beamforming and artificial noise optimization for secure transmissions in MISO-NOMA cognitive radio system with SWIPT," *Electronics*, vol. 9, no. 11, p. 1948, Nov. 2020.

[69] A. P. Prudnikov, Y. A. Brychkov, and O. I. Marichev, *Integrals and Series*. New York, NY, USA: CRC Press, 1986.

LEILA TLEBALDIYEVA received the B.S. degree in communications engineering from Carleton University, Ottawa, ON, Canada, in 2010, the M.Sc. degree in wireless and optical communications from University College London, London, U.K., in 2012, and the Ph.D. degree from the Department of Computer and Electrical Engineering, Nazarbayev University, Nur-Sultan, Kazakhstan, in 2020. Her research interests include spectrum sensing/sharing, cognitive radio networks with hardware imperfections, and device-to-device communication.

GALYMZHAN NAURYZBAYEV (Senior Member, IEEE) received the B.Sc. and M.Sc. degrees (Hons.) in radio engineering, electronics, and telecommunications from the Almaty University of Power Engineering and Telecommunication, Almaty, Kazakhstan, in 2009 and 2011, respectively, and the Ph.D. degree in wireless communications from The University of Manchester, U.K., in 2016. From 2016 to 2018, he held several academic and research positions with Nazarbayev University, Kazakhstan, the L. N. Gumilyov Eurasian National University, Kazakhstan, and Hamad Bin Khalifa University, Qatar. In 2019, he joined as an Assistant Professor at Nazarbayev University. His research interests include wireless communication systems, with particular focus on reconfigurable intelligent surface-enabled communications, multiuser MIMO systems, cognitive radio, signal processing, energy harvesting, visible light communications, NOMA, and interference mitigation. He served as a technical program committee member for numerous IEEE flagship conferences. He serves as a member for the National Research Council of the Republic of Kazakhstan.

SULTANGALI ARZYKULOV (Member, IEEE) received the B.Sc. degree (Hons.) in radio engineering, electronics and telecommunications from Kazakh National Research Technical University after K. I. Satpayev, Almaty, Kazakhstan, in June 2010, the M.Sc. degree in communication engineering from The University of Manchester, Manchester, U.K., in 2013, and the Ph.D. degree in science, engineering and technology from Nazarbayev University, Nur-Sultan, Kazakhstan, in 2019. He is currently a Postdoctoral Scholar with the Computer, Electrical and Mathematical Science and Engineering Division, King Abdullah University of Science and Technology, Saudi Arabia. His research interests include broad areas of wireless communication systems, with a particular focus on cooperative communications, cognitive radio, energy harvesting, interference mitigation, and NOMA. He served as a technical program committee member for numerous IEEE communication society flagship conferences. He acts as a reviewer for several international journals/conferences.

AHMED M. ELTAWIL (Senior Member, IEEE) received the B.Sc. and M.Sc. degrees (Hons.) from Cairo University, Giza, Egypt, in 1997 and 1999, respectively, and the Ph.D. degree from the University of California at Los Angeles, Los Angeles, in 2003. He is currently a Professor with the Computer, Electrical and Mathematical Sciences and Engineering Division, King Abdullah University of Science and Technology (KAUST), which he joined, in August 2019. Prior to that, he was a Professor with the Department of Electrical Engineering and Computer Science, University of California at Irvine, Irvine, in 2005. He is the Founder of the KAUST Communication and Computing System Laboratory, where he is pursuing research interests include the general area of low power digital circuit and signal processing architectures with an emphasis on mobile computing and communication systems and their applications, spanning wireless networks, personal networks, and cyber-physical systems. He is a Senior Member of the National Academy of Inventors. He received several awards, as well as distinguished grants, including the NSF CAREER Grant supporting his research in low power computing and communication systems and the Henry Samueli School of Engineering, University of California at Irvine Innovator of the Year Award for 2021. He has been on the technical program committees and steering committees for workshops, symposia, and conferences in the areas of low power computing, wireless communication system design, and CPS systems.